European Journal of Mechanics B/Fluids 28 (2009) 152–169

Contents lists available at ScienceDirect

European Journal of Mechanics B/Fluids

www.elsevier.com/locate/ejmflu

Numerical study of the generalized cylindrical Couette flow of rarefied gas

E.M. Shakhov [a], V.A. Titarev [b,*]

[a] Bauman Moscow State Technical University, 105005, Moscow, Russia
[b] Cranfield University, MK43 0AL, Cranfield, UK

ARTICLE INFO

Article history:
Received 11 June 2007
Received in revised form 5 April 2008
Accepted 21 April 2008
Available online 8 May 2008

Keywords:
S-model kinetic equation
Cylindrical Couette flow
Stress maximum effect
Implicit TVD scheme

ABSTRACT

We study the cylindrical Couette flow of a rarefied gas between two cylinders in the generalized setup in which the inner of which not only rotates but also slides along its axis. The analysis is based on the numerical solution of the S-model kinetic equation. The influence of ratio of cylinder radiuses, velocities of the inner cylinder and Knudsen number on shear stresses, mass-flow rates as well as macroscopic parameters is investigated in the broad range of Knudsen numbers.

1. Introduction

The plane Couette flow of a rarefied gas between two plates is a classical problem of fluid dynamics. Its axisymmetric extension is given by the flow between moving cylinders and is of not only theoretical but also practical interest, e.g. movement of a long train in a tunnel and of a torus inside a coaxial torus, etc. Assuming that the temperatures of cylinders are equal, the solution of the problem is defined by four parameters: Knudsen number, ratio of radiuses and velocities of longitudinal and rotational movement. Each of these parameters may have a significant influence on the solution pattern.

Most of the existing literature on the kinetic analysis of the problem is devoted to the study of Knudsen-number dependence of macroscopic parameters of the flow in the case of pure rotation for the fixed ratio of the cylinder radiuses, see e.g. [1–4]. The influence of the sliding velocity of the inner cylinder and the ratio of cylinder radiuses has so far been studied only in the case of purely longitudinal cylindrical Couette flow [5]. Some interesting effects have been observed, such as the stress maximum effect for sufficiently large sliding velocities.

The basic goal of present work is to study the cylindrical Couette problem in the generalized formulation in which the inner cylinder both slides along its axis and rotates. Arbitrary ratios of cylinder radiuses are allowed. The dependence of macroscopic parameters, stresses and mass flow rates on Knudsen number and ratio of cylinder radiuses is studied for the three flow patterns: pure longitudinal, pure rotational and generalized, in which the inner cylinder both rotates and slides. The problem is investigated in the whole range of Knudsen numbers and cylinder velocities by solving numerically the model kinetic equation with the S-model collision integral [6,7]. In order to achieve accurate results with the minimal computational cost we use an implicit second-order TVD method, conservative with the respect to the collision integral [8]. Exact analytical solutions are provided for the limiting cases of free-molecular and continuum flows, including asymptotical expressions for small and large gaps between cylinders. The linearized equation is considered for the case of the slow movement of the inner cylinder.

2. Nonlinear problem

2.1. Basic setup

We consider a steady-state rarefied monatomic gas flow between two infinite coaxial cylinders with radii r_1 and r_2. We define radius ratio as $\varepsilon = r_1/r_2 < 1$. The outer cylinder is at rest. The gas flows due to the motion of the inner cylinder which travels along the symmetry axis at a constant velocity U_z and rotates with a constant angle velocity Ω. On the surfaces of the cylinders a constant temperature T_w (the same for both cylinders) is maintained. The momenta and energies of the incident molecules are totally accommodated by the cylinder surfaces and diffusely reflected with the equilibrium distribution functions at the given temperature T_w. The radial gas velocity component is equal to zero.

We introduce the cylindrical coordinate system (r, ϕ, z), where the z axis coincides with the axis of the cylinders, r is the dis-

* Corresponding author.
E-mail addresses: shakhov@ccas.ru (E.M. Shakhov), v.a.titarev@cranfield.ac.uk, titarev@mail.ru (V.A. Titarev).

0997-7546/$ – see front matter
doi:10.1016/j.euromechflu.2008.04.003

tance from this axis, and ϕ is the azimuthal coordinate. The axisymmetric state of the rarefied gas, which is independent of z, is determined by the molecular velocity distribution function $f(t, r, \xi_r, \xi_\phi, \xi_z)$, where ξ_r, ξ_ϕ and ξ_z are the orthogonal components of the velocity vector in the radial, azimuthal, and axial directions, respectively. In velocity space we also introduce a cylindrical coordinate system with the axis parallel to the z axis. We will denote by ζ the velocity component in a plane perpendicular to the axis of the cylinders and by ω the angle between this component and the radial direction outward from the symmetry axis so that $\xi_r = \zeta\cos\omega$, $\xi_\phi = \zeta\sin\omega$.

The problem is studied in nondimensional variables, obtained by normalizing the spatial coordinate r, velocity $\boldsymbol{\xi}$, density n, temperature T, viscosity μ, heat flux $\boldsymbol{q}$ and distribution function f by the following quantities, respectively,

$$r_1, \quad \sqrt{2RT_w}, \quad n_0, \quad T_w, \quad \frac{5}{16} m n_0 \sqrt{2\pi RT_w}\lambda_0,$$
$$m n_0 (2RT_w)^{3/2}, \quad n_0 (2RT_w)^{-3/2}.$$

Here, n_0 is the mean density of the gas between the cylinders:

$$n_0 = \frac{2}{r_2^2 - r_1^2}\int_{r_1}^{r_2} r n(r)\, dr, \tag{1}$$

m is the molecular mass, R is the gas constant, λ_0 is the free path in the gas at rest with density n_0 and temperature T_w. Although in the nondimensional variables the radius of the inner cylinder is equal to unity, below the notation r_1 is retained for convenience of presentation. In what follows, we will denote the nondimensional quantities by the same letters as the corresponding dimensional ones.

2.2. S-model kinetic equation

We will assume that the distribution function $f(t, r, \xi_r, \xi_\phi, \xi_z)$ satisfies the Boltzmann equation with the S-model collision operator [6,7]. In the cylindrical coordinate system this equation is written as

$$\zeta\cos\omega\frac{\partial f}{\partial r} - \frac{\zeta\sin\omega}{r}\frac{\partial f}{\partial \omega} = \nu(f^+ - f),$$
$$\nu = \frac{8}{5\sqrt{\pi}}\frac{nT}{\mu}\frac{1}{Kn},$$
$$f^+ = f_M\left(1 + \frac{4}{5}(1-Pr)S_\alpha c_\alpha\left(c^2 - \frac{5}{2}\right)\right),$$
$$f_M = \frac{n}{(\pi T)^{3/2}}\exp\left(-c^2\right),$$
$$\boldsymbol{S} = (S_r, S_\phi, S_z) = \frac{2(q_r, q_\phi, q_r)}{nT^{3/2}},$$
$$\boldsymbol{v} = (v_r, v_\phi, v_z) = (\xi_r, \xi_\phi - u_\phi, \xi_z - u_z),$$
$$\boldsymbol{c} = \frac{\boldsymbol{v}}{\sqrt{T}}. \tag{2}$$

Here, $Kn = \lambda_0/r_1$ is the Knudsen number, which characterizes the degree of gas rarefaction; ν is the collision frequency, $Pr = 2/3$ is the Prandtl number.

The number density n, gas temperature T, components of gas velocity $\boldsymbol{u} = (0, u_\phi, u_z)$ and heat flux $\boldsymbol{q} = (q_r, q_\phi, q_z) = (q_1, q_2, q_3)$ are given as the integrals of the velocity distribution function with respect to molecular velocity:

$$n = \int f\, d\xi, \qquad \boldsymbol{u} = \frac{1}{n}\int \boldsymbol{\xi} f\, d\boldsymbol{\xi}, \qquad \frac{3}{2}nT + nu^2 = \int \xi^2 f\, d\boldsymbol{\xi},$$
$$\boldsymbol{q} = \frac{1}{2}\int \boldsymbol{v} v^2 f\, d\boldsymbol{\xi}, \qquad d\boldsymbol{\xi} = d\xi_r\, d\xi_\phi\, d\xi_z = \zeta\, d\zeta\, d\omega\, d\xi_z \tag{3}$$

For the shear stresses we have:

$$P_{r\phi} = \int v_r v_\phi f\, d\boldsymbol{\xi}, \qquad P_{rz} = \int v_r v_z f\, d\boldsymbol{\xi}.$$

The boundary conditions in the problem are set as follows. On the surface of the cylinders, we use the diffuse reflection of molecules with complete thermal accommodation to the surface temperature:

$$r = r_1, \quad \xi_r > 0: \quad f_1 = \frac{n_1}{\pi}\exp\left(-\xi_r^2 - (\xi_\phi - U_\phi)^2 - (\xi_z - U_z)^2\right),$$
$$r = r_2, \quad \xi_r < 0: \quad f_2 = \frac{n_2}{\pi}\exp\left(-\zeta^2 - \xi_z^2\right) \tag{4}$$

where $U_\phi = \Omega r_1$ and is taken into account that in the nondimensional variables $T_w \equiv 1$. Densities of reflected molecules n_1, n_2 are found from the impermeability condition:

$$n_1 = -2\sqrt{\pi}\int_{-\infty}^{0}\xi_r\, d\xi_r \int f\, d\xi_\phi\, d\xi_z,$$
$$n_2 = +2\sqrt{\pi}\int_{0}^{\infty}\xi_r\, d\xi_r \int f\, d\xi_\phi\, d\xi_z.$$

In addition to the above boundary conditions, the number of particles per unit cylinder length is assumed to be constant. In nondimensional variables, this condition has the form $n_0 = 1$, where the mean particle density n_0 is defined by (1).

2.3. Simplification of the problem

Following [9], we reduce the problem dimension by going over from the distribution function to its integral $\boldsymbol{g}$ by means of the formula

$$\boldsymbol{g} = \begin{pmatrix} g_1 \\ g_2 \\ g_3 \\ g_4 \end{pmatrix} = \int_{-\infty}^{+\infty}\begin{pmatrix} 1 \\ \xi_z \\ \xi_z^2 \\ \xi_z^3 \end{pmatrix} f\, d\xi_z.$$

The kinetic equation for $\boldsymbol{g}$ in the cylindrical coordinate system is written as:

$$\zeta\cos\omega\frac{\partial \boldsymbol{g}}{\partial r} - \frac{\zeta\sin\omega}{r}\frac{\partial \boldsymbol{g}}{\partial \omega} = \nu(\boldsymbol{g}^+ - \boldsymbol{g}) \tag{5}$$

where the components of $\boldsymbol{g}^+$ are given by

$$\boldsymbol{g}^+ = g_M\begin{pmatrix} \left(1 + Z(S_r c_r + S_\phi c_\phi)\left(c_r^2 + c_\phi^2 - 2\right)\right) \\ \frac{1}{2}\sqrt{T}ZS_z\left(c_r^2 + c_\phi^2 - 1\right) + u_z G_1 \\ \frac{1}{2}T\left(1 + Z(S_r c_r + S_\phi c_\phi)\left(c_r^2 + c_\phi^2 - 1\right)\right) + 2u_z G_2 - u_z^2 G_1 \\ \frac{3}{4}T^{3/2}ZS_z\left(c_r^2 + c_\phi^2\right) + 3u_z^3 G_3 - 3u_z^2 G_2 + u_z^3 G_1 \end{pmatrix}$$

where

$$g_M = \frac{n}{\pi T}\exp\left(-c_r^2 - c_\phi^2\right), \qquad Z = \frac{4}{5}(1 - Pr).$$

The expressions for macroscopic parameters (3) can be rewritten in terms of $\boldsymbol{g}$ as

$$\left(n, nu_\phi, nu_z, \frac{3}{2}nT + nu_\phi^2 + nu_z^2\right)$$
$$= \int_{-\pi}^{\pi}\int_{0}^{\infty}\left(g_1, \xi_\phi g_1, g_2, \zeta^2 g_1 + g_3\right)\zeta\, d\zeta\, d\omega,$$

$$(q_r, q_\phi) = \frac{1}{2}\int_{-\pi}^{\pi}\int_0^\infty (\xi_r, v_\phi)\left[\left(\xi_r^2 + v_\phi^2\right)g_1 - 2u_z g_2 + g_3\right]\zeta\, d\zeta\, d\omega,$$

$$q_z = nu_z^3 + \frac{1}{2}\int_{-\pi}^{\pi}\int_0^\infty \left(\left(\xi_r^2 + v_\phi^2\right)(g_2 - u_z g_1) + (g_4 - 3u_z g_3)\right)\zeta\, d\zeta\, d\omega. \tag{6}$$

Note that, if $|U_z| > 0$, the longitudinal heat flux q_z is also nonzero [10]; therefore, we have to use g_4. The shear stresses $P_{r\phi}$, P_{rz} are given by

$$P_{r\phi} = \int_{-\pi}^{\pi}\int_0^\infty \xi_r\xi_\phi g_1\zeta\, d\zeta\, d\omega, \qquad P_{rz} = \int_{-\pi}^{\pi}\int_0^\infty \xi_r g_2\zeta\, d\zeta\, d\omega.$$

Boundary conditions (4) take the following form:

$$r = r_1, \quad \xi_r > 0: \quad \boldsymbol{g}_{w1} = \frac{1}{\pi}n_{w1}e^{-\xi_r^2-(\xi_\phi-U_\phi)^2}\left(1, U_z, \frac{1}{2}+U_z^2, \frac{3}{2}U_z + 2U_z^3\right)^T,$$

$$r = r_2, \quad \xi_r < 0: \quad \boldsymbol{g}_{w2} = \frac{1}{\pi}n_{w2}e^{-\zeta^2}\left(1, 0, \frac{1}{2}, 0\right)^T \tag{7}$$

with

$$n_{w1} = -2\sqrt{\pi}\int_{-\infty}^{0}\xi_r\, d\xi_r \int g_1\, d\xi_\phi,$$

$$n_{w2} = +2\sqrt{\pi}\int_{0}^{\infty}\xi_r\, d\xi_r \int g_1\, d\xi_\phi.$$

2.4. Integral relations

Multiplying the kinetic equation (2) by ξ_ϕ, ξ_z and $\zeta^2 + \xi_z^2$ and integrating over the entire velocity space, we obtain the equations:

$$\frac{dP_{r\phi}}{dr} + \frac{2}{r}P_{r\phi} = 0, \quad \frac{dP_{rz}}{dr} + \frac{1}{r}P_{rz} = 0, \quad \frac{dE_r}{dr} + \frac{1}{r}E_r = 0$$

where E_r is the energy flux in the radial direction. Integration gives three important integral relations:

$$r^2 P_{r\phi} = \text{const} = \text{A}, \quad rP_{rz} = \text{const} = \text{B}, \quad rE_r = \text{const} = \text{C}. \tag{8}$$

The constants A, B and C depend on the degree of gas rarefaction, on the ratio of r_1 to r_2, and on the nondimensional velocities U_z and U_ϕ. Conditions (8) can also be used to control the accuracy of the computations.

Interesting integral characteristics of the problem considered are the averaged gas velocities in longitudinal and azimuthal direction which with account for the normalization condition (1) are given by the integrals

$$W_\phi = \frac{2}{r_2^2 - r_1^2}\int_{r_1}^{r_2} nu_\phi r\, dr, \qquad W_z = \frac{2}{r_2^2 - r_1^2}\int_{r_1}^{r_2} nu_z r\, dr.$$

The corresponding gas flow-rates per unit time

$$Q_\phi = \pi\left(r_2^2 - r_1^2\right)W_\phi, \quad Q_z = \pi\left(r_2^2 - r_1^2\right)W_z.$$

In the classical Couette flow between parallel plates, $W_z = U_z/2$ irrespective of the Knudsen number. In the case considered, the mean gas velocity depends on both the rarefaction degree and the radius ratio.

3. Limiting cases

3.1. Free-molecular flow

We first study the free-molecular case $Kn = \infty$. The kinetic equation (5) has a general solution

$$\boldsymbol{g}(r, \zeta, \omega) = \boldsymbol{g}_\infty(r\sin\omega, \zeta)$$

where $\boldsymbol{g}_\infty$ is an arbitrary function of its arguments the form of which is defined by the boundary conditions. We therefore obtain the following expressions:

$$\boldsymbol{g}(r, \zeta, \omega) = \begin{cases} \boldsymbol{g}_{w1}, & -\omega_0 \leqslant \omega \leqslant \omega_0, \\ \boldsymbol{g}_{w2}, & -\pi \leqslant \omega \leqslant -\omega_0 \text{ or } \omega_0 \leqslant \omega \leqslant \pi, \end{cases}$$

where $\omega_0 = \omega_0(r) = \arcsin(r_1/r)$; boundary values $\boldsymbol{g}_{w1}$, $\boldsymbol{g}_{w2}$ are defined in (7); the densities of the reflected molecules $n_w = n_{w1} = n_{w2}$ are found from the condition (1). Density, temperature and components of velocity are given by

$$n\left(1, u_\phi, u_z, \frac{3}{2}T + u_\phi^2 + u_z^2\right) = \frac{1}{\pi}n_w\left(\pi - \omega_0, 0, 0, \frac{3}{2}(\pi - \omega_0)\right) + \frac{1}{\pi}n_w e^{-U_\phi^2}\int_{-\omega_0}^{\omega_0}\int_0^\infty e^{-\zeta^2 + 2rU_\phi\zeta\sin\omega} \times \left(1, \zeta\sin\omega, U_z, \zeta^2 + U_z^2 + \frac{1}{2}\right)\zeta\, d\zeta\, d\omega. \tag{9}$$

The expressions for the heat fluxes are quite bulky and are thus omitted. The shear stresses are given by

$$(P_{r\phi}, P_{rz}) = \frac{1}{\pi}n_w e^{-U_\phi^2}\int_{-\omega_0}^{\omega_0}\int_0^\infty (\zeta\sin\omega, U_z)e^{-\zeta^2 + 2rU_\phi\zeta\sin\omega}\zeta^2\cos\omega\, d\zeta\, d\omega.$$

It is obvious, that in the free-molecular case density, u_ϕ and $P_{r\phi}$ do not depend on the velocity of longitudinal movement U_z, whereas u_z and P_{rz} are linear functions of U_z. In the case of no rotation the integrals can be evaluated exactly and we obtain [5]:

$$n_w = n = 1, \qquad u_z = \frac{\omega_0}{\pi}U_z,$$
$$T = 1 + \frac{2\omega_0}{3\pi}\left(1 - \frac{\omega_0}{\pi}\right)U_z^2, \qquad B = \frac{U_z}{2\sqrt{\pi}}. \tag{10}$$

3.2. Continuum regime

Another limiting case $Kn \to 0$ corresponds to the continuum solution. For small values of the cylinder velocity we can use the incompressible Navier–Stokes equations [11]:

$$\frac{d^2u_\phi}{dr^2} + \frac{1}{r}\frac{du_\phi}{dr} - \frac{u_\phi^2}{r^2} = 0, \qquad \frac{d^2u_z}{dr^2} + \frac{1}{r}\frac{du_z}{dr} = 0.$$

The general solution is given by

$$u_\phi = \alpha_1 r + \frac{\alpha_2}{r}, \qquad u_z = \beta_1\ln r + \beta_2,$$

where unknown constants are found from the boundary conditions. Once the equations are solved with the appropriate boundary conditions, quantities A and B, defined in (8), are computed according to the expressions

$$\text{A}_{\text{NS}} = -\frac{5\sqrt{\pi}}{16}Kn\left(\frac{du_\phi}{dr} - \frac{u_\phi}{r}\right), \qquad \text{B}_{\text{NS}} = -\frac{5\sqrt{\pi}}{16}Kn\left(\frac{du_z}{dr}\right). \tag{11}$$

We consider two types of boundary conditions on the cylinder surfaces: with and without velocity slip. We note that the solution for

the *compressible* Navier–Stokes equations with velocity–slip boundary conditions was obtained in [12]. In the present incompressible case the exact solution is found trivially in the same manner as for the non-slip boundary conditions.

3.2.1. Nonslip boundary conditions

These are the simplest conditions: the gas velocity is zero at $r = r_1$ and $r = r_2$. We then obtain

$$u_\phi = \left(\frac{r_1}{r}\right)\frac{r_2^2 - r^2}{r_2^2 - r_1^2}U_\phi, \qquad u_z = \frac{\ln(r_2/r)}{\ln(r_2/r_1)}U_z,$$
$$\mathrm{A_{NS}} = \frac{5\sqrt{\pi}}{8}\frac{Kn}{1-\varepsilon^2}U_\phi, \qquad \mathrm{B_{NS}} = -\frac{5\sqrt{\pi}}{16}\frac{Kn}{\ln\varepsilon}U_z. \tag{12}$$

The average values of velocities in longitudinal and azimuthal are given by

$$W_{\phi,\mathrm{NS}} = \frac{2\varepsilon(\varepsilon+2)}{3(\varepsilon+1)^2}U_\phi, \qquad W_{z,\mathrm{NS}} = \frac{\varepsilon^2(1-2\ln\varepsilon)-1}{2(1-\varepsilon^2)\ln\varepsilon}U_z.$$

The gas flow-rates per unit time in longitudinal and azimuthal directions take the following form:

$$Q_{\phi,\mathrm{NS}} = 2\pi\frac{2-\varepsilon-\varepsilon^2}{3(\varepsilon+1)\varepsilon}U_\phi, \qquad Q_{z,\mathrm{NS}} = \pi\frac{\varepsilon^2(1-2\ln\varepsilon)-1}{2\varepsilon^2\ln\varepsilon}U_z.$$

In the case of the large gap between cylinders ($\varepsilon \to 0$) we have

$$W_{\phi,\mathrm{NS}} \approx \frac{4}{3}\varepsilon U_\phi, \quad Q_{\phi,\mathrm{NS}} \approx \frac{4\pi}{3\varepsilon}U_\phi,$$
$$W_{z,\mathrm{NS}} \approx -\frac{1}{2\ln\varepsilon}U_z, \quad Q_{z,\mathrm{NS}} \approx -\frac{\pi}{2\varepsilon^2\ln\varepsilon}U_z.$$

In the opposite case ($\varepsilon \to 1$):

$$W_{\phi,\mathrm{NS}} \approx \frac{1}{2}U_\phi, \quad Q_{\phi,\mathrm{NS}} \approx \pi(1-\varepsilon)U_\phi,$$
$$W_{z,\mathrm{NS}} \approx \frac{1}{2}U_z, \quad Q_{z,\mathrm{NS}} \approx \pi(1-\varepsilon)U_z.$$

3.2.2. Velocity–slip boundary conditions

There are several variations of the slip–velocity boundary conditions in the literature [12–15], all of which differ slightly in the coefficient in front of the shear stress. We shall use the particular form from [13], which in the nondimensional variables read as follows:

$$r = r_1: \quad u_\phi = U_\phi + Kn\left(\frac{du_\phi}{dr} - \frac{u_\phi}{r}\right), \quad u_z = U_z + Kn\left(\frac{du_z}{dr}\right),$$
$$r = r_2: \quad u_\phi = -Kn\left(\frac{du_\phi}{dr} - \frac{u_\phi}{r}\right), \quad u_z = -Kn\left(\frac{du_z}{dr}\right).$$

The solution is then given by

$$u_\phi = U_\phi\frac{r_1^2(r_2{}^3 - r^2 r_2 + 2r^2 Kn)}{(2(r_2^3 + r_1^3)Kn + r_1 r_2(r_2^2 - r_1^2))r},$$
$$u_z = U_z\frac{\ln(r_2/r) + Kn/r_2}{\ln(r_2/r_1) + Kn/r_1 + Kn/r_2}. \tag{13}$$

Explicit expressions for stresses, mass fluxes and averaged velocities are obtained in the same way as for the nonslip boundary conditions and are omitted here to save space. We remark that obviously, A_{NS} and B_{NS} are no longer linear functions of Kn. Also, mass fluxes and averaged velocities now depend on Kn.

4. Linearized problem

When the velocity of the inner cylinders is small ($U_\phi, U_z \ll 1$), the perturbations are small and the kinetic equation can be linearized around the rest state. Then the main disturbances correspond to the gas velocity and friction; the perturbations of pressure, temperature, density and the heat flux in the radial direction are small quantities of second order in the cylinder velocity and can be neglected. However, the heat fluxes in the flow directions q_ϕ, q_z are of first-order in the cylinder velocity and should therefore be accounted for [16,17]. Surprisingly, in the free-molecular case $Kn = \infty$ these two fluxes are also of higher than first-order terms in the cylinder velocity. For the plane Couette flow this fact can be trivially shown by the exact integration of the kinetic equation [18]. It is only when the Knudsen number is finite do they become important.

Thus, in the linear approximation density and temperature are constant:

$$n = T = T_w = 1.$$

We will denote the Maxwellian function at rest with the subscript "0" and the perturbation of the distribution function by h. Then for the distribution function f, the locally Maxwellian function, and the boundary condition we can write

$$f = f_0(1+h), \quad h = h(r,\zeta,\omega,\xi_z), \quad f_0 = (\pi)^{-3/2}\exp\left(-\xi^2\right),$$
$$f^+ = f_0\Bigg(1 + 2u_\phi\xi_\phi + 2u_z\xi_z + \frac{8}{5}(1-Pr)(q_\phi\xi_\phi + q_z\xi_z)\left(\xi_r^2 + \xi_\phi^2 + \xi_z^2 - \frac{5}{2}\right)\Bigg),$$
$$f_{w1} = f_0(1 + 2U_\phi\xi_\phi + 2U_z\xi_z), \quad f_{w2} = f_0. \tag{14}$$

Substituting expressions (14) into (2), retaining terms of the order of U_z, U_ϕ, and making the necessary cancellations, we obtain the following equation for the function h:

$$\zeta\cos\omega\frac{\partial h}{\partial r} - \frac{\zeta\sin\omega}{r}\frac{\partial h}{\partial\omega} = \nu_0(h^+ - h), \quad \nu_0 = \frac{8}{5\sqrt{\pi}}\frac{1}{Kn},$$
$$h^+ = 2u_\phi\xi_\phi + 2u_z\xi_z + \frac{8}{5}(1-Pr)(q_\phi\xi_\phi + q_z\xi_z)\left(\xi_r^2 + \xi_\phi^2 + \xi_z^2 - \frac{5}{2}\right). \tag{15}$$

Boundary conditions follow from (4):

$$r = r_1, \quad \xi_r > 0: \quad h_{w1} = 2U_\phi\xi_\phi + 2U_z\xi_z,$$
$$r = r_2, \quad \xi_r < 0: \quad h_{w2} = 0.$$

In the linearized problem the normalization condition (1) is satisfied identically.

Similar to the nonlinear case, the linearized equation (15) can be simplified by passing from h to its integrals $\boldsymbol{\psi}$:

$$\boldsymbol{\psi} = \begin{pmatrix}\psi_1\\ \psi_2\\ \psi_3\\ \psi_4\end{pmatrix} = \frac{1}{\sqrt{\pi}}\int_{-\infty}^{\infty}\begin{pmatrix}1\\ \xi_z\\ \xi_z^2\\ \xi_z^3\end{pmatrix}e^{-\xi_z^2}h\,d\xi_z.$$

The resulting equation for $\boldsymbol{\psi}$ reads

$$\zeta\cos\omega\frac{\partial\boldsymbol{\psi}}{\partial r} - \frac{\zeta\sin\omega}{r}\frac{\partial\boldsymbol{\psi}}{\partial\omega} = \nu_0(\boldsymbol{\psi}^+ - \boldsymbol{\psi}), \tag{16}$$

where

$$\boldsymbol{\psi}^+ = \begin{pmatrix}2u_\phi\xi_\phi + 2Zq_\phi\xi_\phi\left(\zeta^2 - 2\right),\\ u_z + Zq_z\left(\zeta^2 - 1\right)\\ u_\phi\xi_\phi + Zq_\phi\xi_\phi\left(\zeta^2 - 1\right)\\ \frac{3}{2}u_z + \frac{3}{2}Zq_z\zeta^2\end{pmatrix}.$$

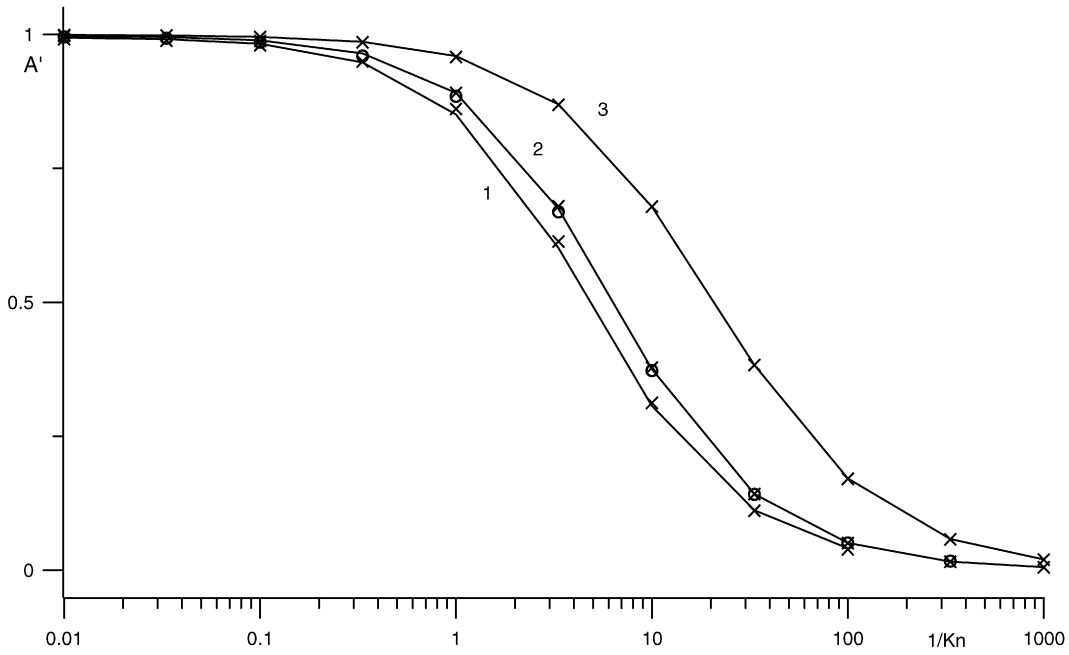

Fig. 1. Normalized shear stress A' for $U_\phi = U_z = 1/2$, obtained by the nonlinear kinetic equation (5). Solid line – general movement, circles – pure rotation, crosses – linearized solution. Curves 1, 2, 3 correspond to $\varepsilon = 0.1,\ 0.5,\ 0.9$, respectively.

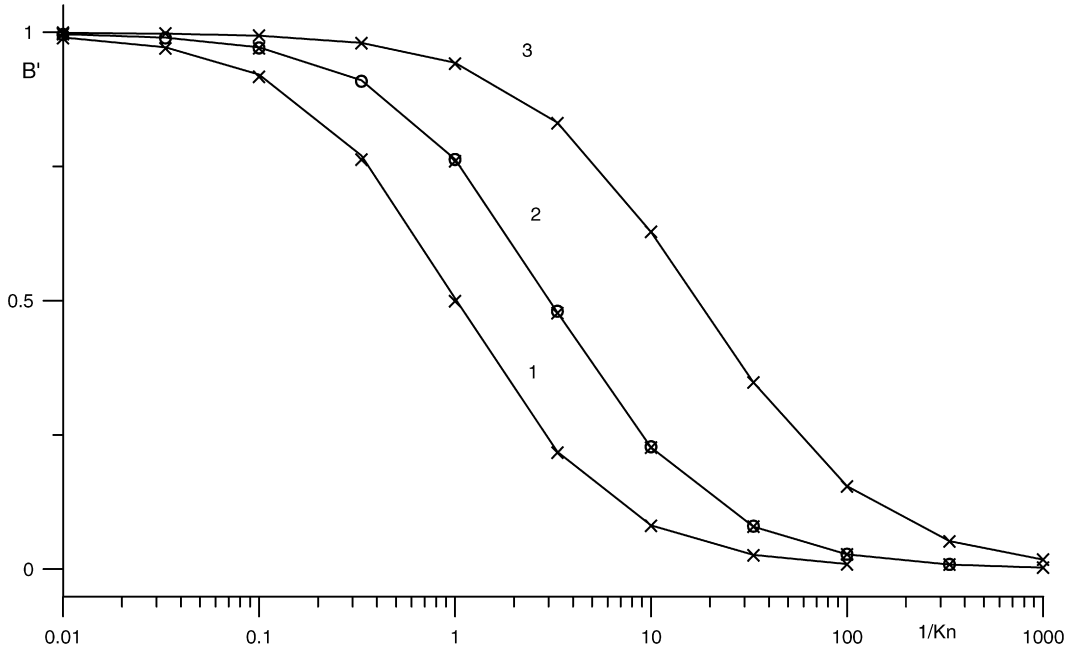

Fig. 2. Normalized shear stress B' for $U_\phi = U_z = 1/2$, obtained by the nonlinear kinetic equation (5). Solid line – general movement, circles – pure sliding, crosses – linearized solution. Curves 1, 2, 3 correspond to $\varepsilon = 0.1,\ 0.5,\ 0.9$, respectively.

The boundary conditions for $\boldsymbol{\psi}$ are given by

$$r = r_1, \quad \xi_r > 0: \quad \boldsymbol{\psi}_{w1} = \left(2U_\phi \xi_\phi, U_z, U_\phi \xi_\phi, \frac{3}{2}U_z\right)^T,$$
$$r = r_2, \quad \xi_r < 0: \quad \boldsymbol{\psi}_{w2} = \mathbf{0}. \tag{17}$$

Components of gas velocity and shear stresses are now given by

$$u_\phi = \frac{1}{\pi}\int_{-\pi}^{\pi}\int_0^\infty \zeta^2 e^{-\zeta^2}\psi_1 \sin\omega\, d\zeta\, d\omega,$$
$$u_z = \frac{1}{\pi}\int_{-\pi}^{\pi}\int_0^\infty \zeta e^{-\zeta^2}\psi_2\, d\zeta\, d\omega,$$
$$P_{r\phi} = \frac{1}{\pi}\int_{-\pi}^{\pi}\int_0^\infty \zeta^3 e^{-\zeta^2}\psi_1 \cos\omega \sin\omega\, d\zeta\, d\omega,$$
$$P_{rz} = \frac{1}{\pi}\int_{-\pi}^{\pi}\int_0^\infty \zeta^2 e^{-\zeta^2}\psi_2 \cos\omega\, d\zeta\, d\omega. \tag{18}$$

Taking into account that the shear stresses are of first order in the cylinder velocity and thus their products with components

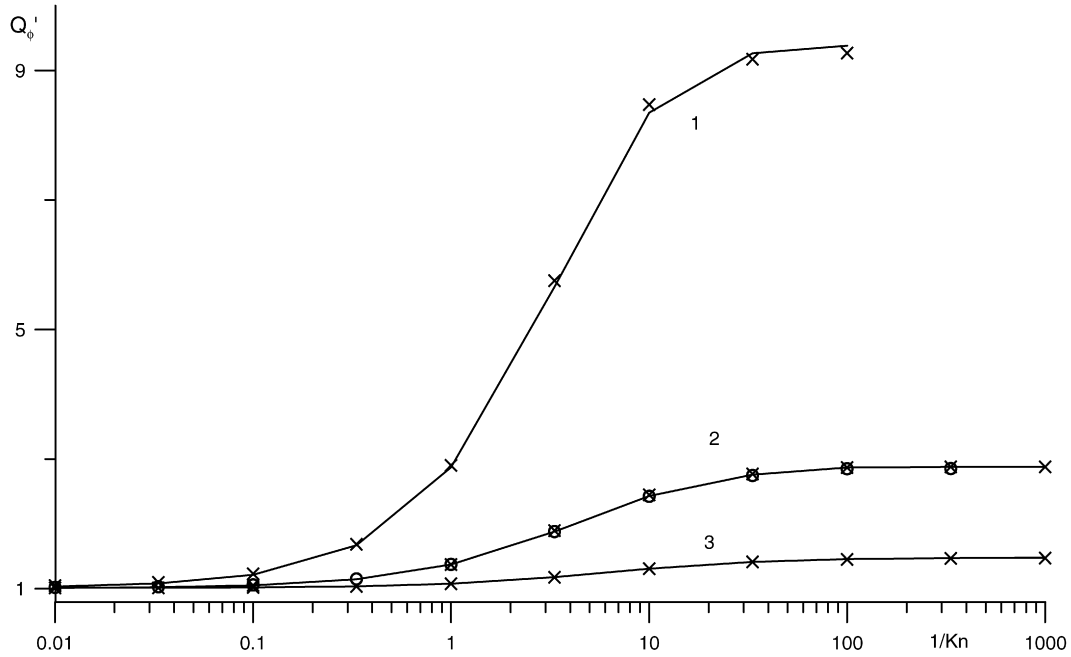

Fig. 3. Normalized mass-flow rate Q'_ϕ for $U_\phi = U_z = 1/2$, obtained by the nonlinear kinetic equation (5). Solid line – general movement, circles – pure rotation, crosses – linearized solution. Curves 1, 2, 3 correspond to $\varepsilon = 0.1,\ 0.5,\ 0.9$, respectively.

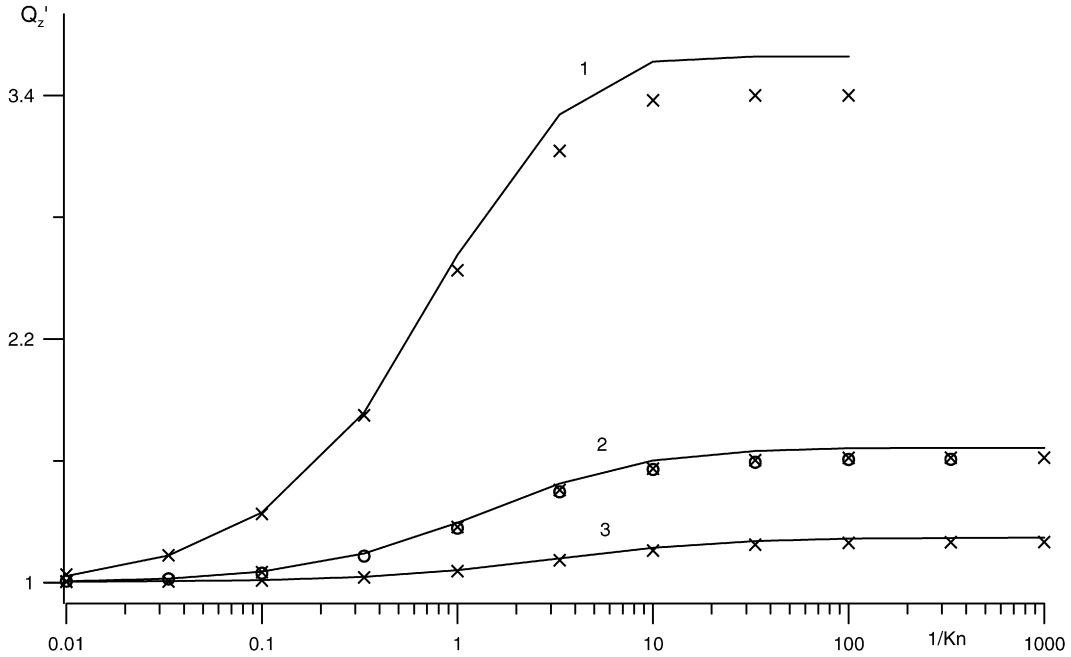

Fig. 4. Normalized mass-flow rate Q'_z for $U_\phi = U_z = 1/2$, obtained by the nonlinear kinetic equation (5). Solid line – general movement, circles – pure sliding, crosses – linearized solution. Curves 1, 2, 3 correspond to $\varepsilon = 0.1,\ 0.5,\ 0.9$, respectively.

of gas velocity can be neglected, the heat fluxes are given by the following expressions:

$$q_\phi = -\frac{5}{4}u_\phi + \frac{1}{2}\int \left\{ v_\phi \psi_3 + \left[\zeta^2 v_\phi - 2\xi_\phi^2 u_\phi\right]\psi_1 \right\} e^{-\eta^2}\,\zeta\,d\zeta\,d\omega,$$

$$q_z = -\frac{5}{4}u_z + \frac{1}{2}\int \left\{ \psi_4 - u_z\psi_3 + \zeta^2\psi_2 - u_z\zeta^2\psi_1 \right\} e^{-\zeta^2}\,\zeta\,d\zeta\,d\omega. \quad (19)$$

It is obvious from Eqs. (16)–(19) that the linearized problem decomposes into two separate problems corresponding to pure rotation and pure longitudinal movement of the inner cylinder. These problems can be solve separately. Moreover, from the structure of the boundary conditions (17) we conclude that the solutions are linear functions of the velocity of the inner cylinder:

$$\psi_1(U_\phi) = U_\phi\psi_1(1), \qquad \psi_2(U_z) = U_z\psi_2(1),$$
$$\psi_3(U_\phi) = U_\phi\psi_3(1), \qquad \psi_4(U_z) = U_z\psi_4(1). \quad (20)$$

It is therefore sufficient to compute the solution for the particular case $U_\phi = U_z = 1$ only; for other values of U_z, U_ϕ one can use simple relation (20).

The free-molecular solution of the linearized problem is constructed in the same way as for the complete nonlinear problem.

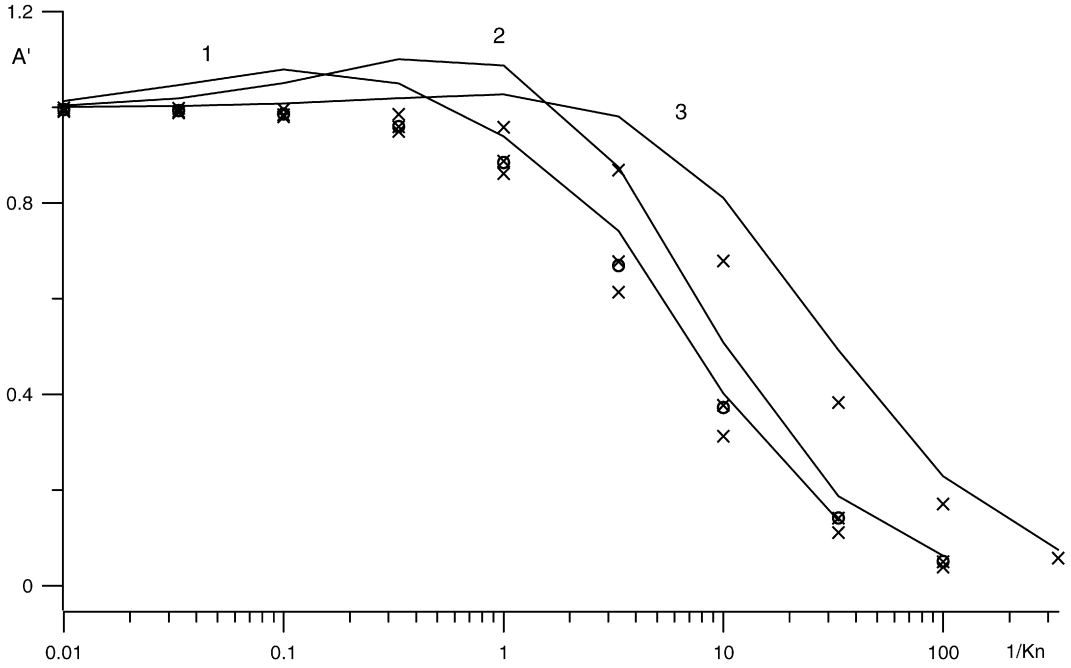

Fig. 5. Normalized shear stress A' for $U_\phi = 1/2$, $U_z = 4$, obtained by the nonlinear kinetic equation (5). Notation is as on Fig. 1.

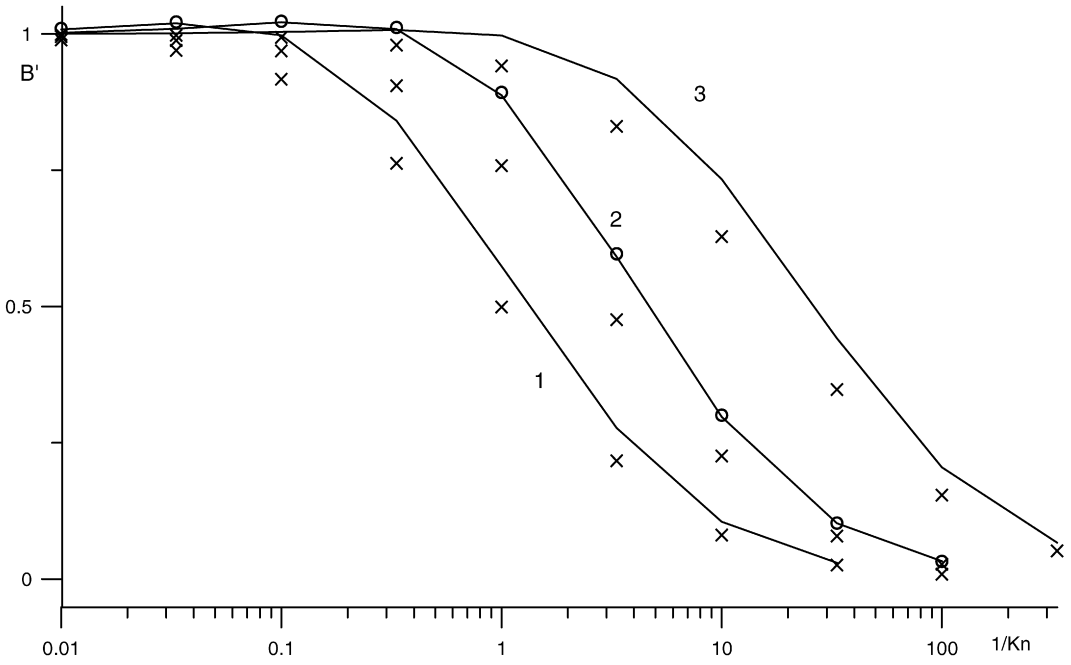

Fig. 6. Normalized shear stress B' for $U_\phi = 1/2$, $U_z = 4$, obtained by the nonlinear kinetic equation (5). Notation is as on Fig. 2.

In particular, expressions for B, Q_z and W_z are identical to those corresponding to the case of no rotation and are given by (10).

5. Numerical method

For intermediate Knudsen numbers $0 < Kn < \infty$ or large velocities of the inner cylinder the solution to the problem is obtained by solving the kinetic equation in the time-dependent form numerically, by marching in time to the steady state. The numerical method consists of a second-order implicit Godunov-type scheme [19,20] and a special procedure of computing the macroscopic parameters in the S-model, which ensures the conservation property with respect to the collision integral [21,22] The resulting numerical method works well across the whole range of Knudsen numbers from the free-molecular limit to the continuum regime $Kn \ll 1$. The implicit temporal discretization scheme used in the method speeds up the convergence to steady state by allowing the use of large time steps.

5.1. Implicit Godunov-type TVD scheme

We rewrite the kinetic equation for $\boldsymbol{g}$ in the following conservative form [23]:

$$\frac{\partial}{\partial t}(r\boldsymbol{g}) = -\frac{\partial}{\partial r}(\boldsymbol{g} r\zeta\cos\omega)$$

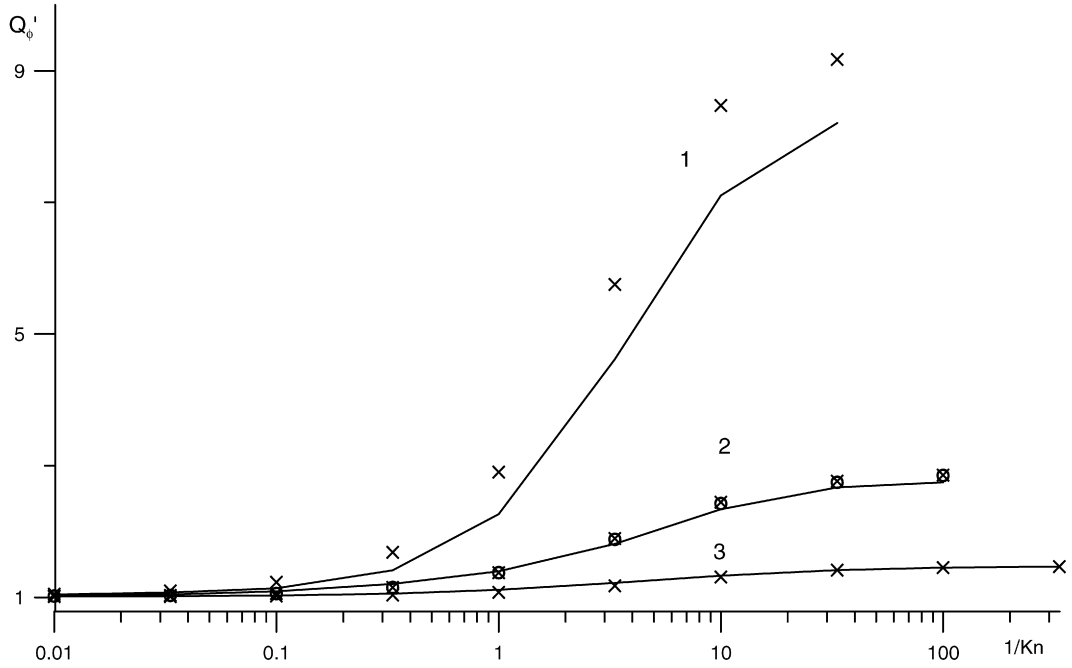

Fig. 7. Normalized mass-flow rate Q'_ϕ for $U_\phi = 1/2$, $U_z = 4$, obtained by the nonlinear kinetic equation (5). Notation is as on Fig. 3.

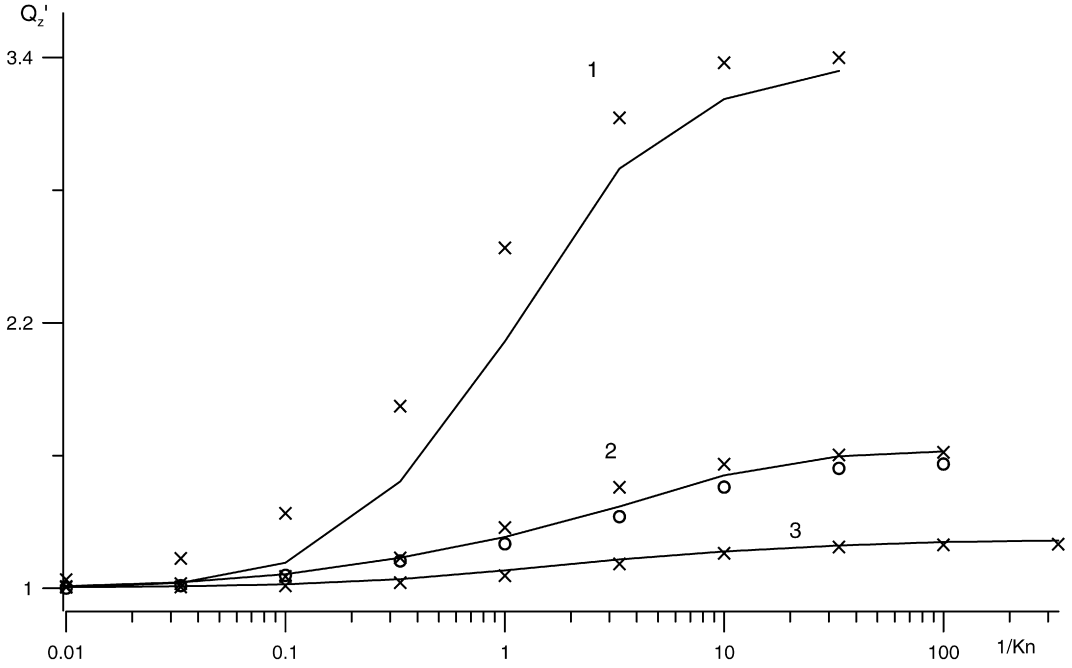

Fig. 8. Normalized mass-flow rate Q'_z for $U_\phi = 1/2$, $U_z = 4$, obtained by the nonlinear kinetic equation (5). Notation is as on Fig. 4.

$$+\frac{\partial}{\partial\omega}(\boldsymbol{g}\zeta\sin\omega)+r\boldsymbol{H},\quad \boldsymbol{H}=\nu(\boldsymbol{g}^{+}-\boldsymbol{g}). \tag{21}$$

Let us define $\Delta t = t^{n+1} - t^n$, $\boldsymbol{g}^n = \boldsymbol{g}(t^n, r, \omega, \zeta)$, $\boldsymbol{\delta} = r(\boldsymbol{g}^{n+1} - \boldsymbol{g}^n)$. A fully implicit Godunov-type scheme for kinetic equation (21) can be written in the following form [5,19,20]:

$$\left(\frac{1}{\Delta t}+\zeta\frac{\partial}{\partial r}\cos\omega-\left(\frac{\zeta}{r}\right)\frac{\partial}{\partial\omega}\sin\omega+\nu\right)\boldsymbol{\delta}=\boldsymbol{K}^n,$$

$$\boldsymbol{K}^n=-\frac{\partial}{\partial r}(r\zeta\cos\omega\boldsymbol{g})^n+\frac{\partial}{\partial\omega}(\zeta\sin\omega\boldsymbol{g})^n+r\boldsymbol{H}^n. \tag{22}$$

Next in variables r, ω we introduce a finite-volume mesh of $N_r \times N_\omega$ cells with cell centers r_i, ω_j; the spatial mesh is refined toward the surfaces of the cylinders. With respect to ζ we use a uniform mesh with nodes ζ_k, $k = 0, \ldots, N_\zeta$, and cell size $\Delta\zeta$. The range of ω is divided into four subdomains depending on the sign of the molecular velocity components ξ_r, ξ_ϕ: $-\pi + m\pi/2 \leqslant \omega \leqslant -\pi/2 + m\pi/2$, where $m = 0, \ldots, 3$. For each subdomain, the derivatives with respect to r and ω on the left-hand side of (22) are approximated by first-order accurate upwind differences. As a result, the distribution function at a new time level is determined according to a running scheme. For example, for $m = 1$ and a fixed k the computation is performed from left to right with respect to r according to the formula

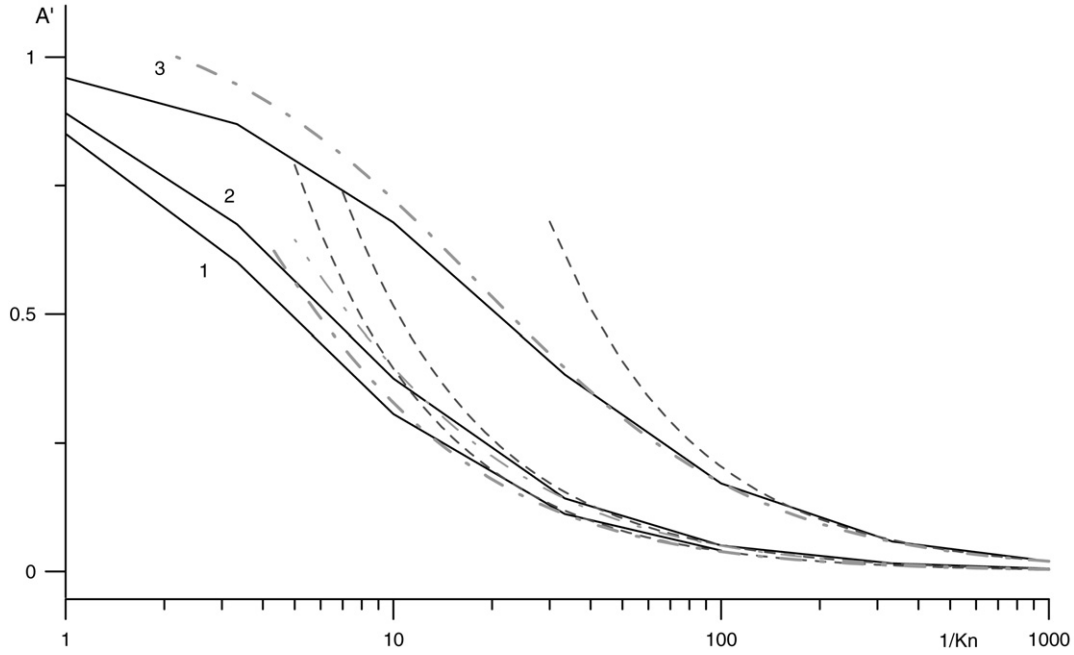

Fig. 9. Normalized shear stress A' for $U_\phi = U_z = 1/2$. Solid line – solution of the nonlinear kinetic equation (5), dashed line – continuum solution with non-slip boundary conditions (12), dash-dotted line – continuum solution with velocity–slip boundary conditions (13). Curves 1, 2, 3 correspond to $\varepsilon = 0.1$, 0.5, 0.9, respectively.

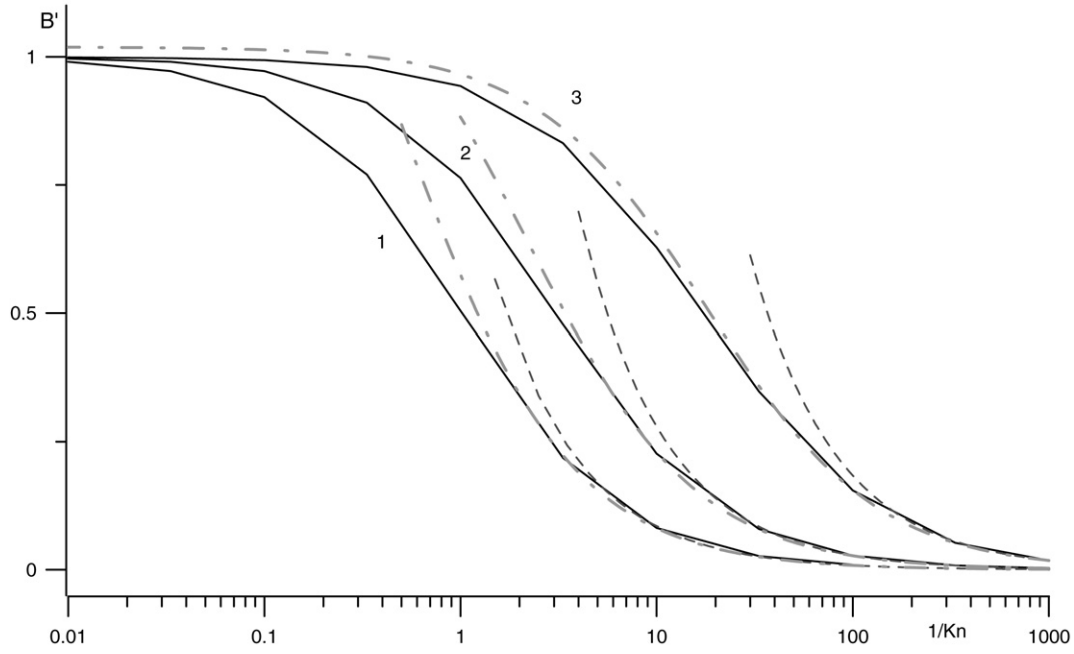

Fig. 10. Normalized shear stress B' for $U_\phi = U_z = 1/2$. Notation is as on Fig. 9.

$$\left(\frac{1}{\Delta t} + B_{ijk} + C_{ij-1,k} + \nu_i\right)\boldsymbol{\delta}_{ijk} = B_{ijk}\boldsymbol{\delta}_{i-1,jk} + C_{ij-1,k}\boldsymbol{\delta}_{ij-1,k} + \boldsymbol{K}^n_{ijk}, \tag{23}$$

where

$$\boldsymbol{\delta}_{ijk} = r_i\left(\boldsymbol{g}^{n+1}_{ijk} - \boldsymbol{g}^n_{ijk}\right), \qquad B_{ijk} = \frac{\zeta_k \cos\omega_j}{r_i - r_{i-1}}, \qquad C_{ijk} = -\frac{\zeta_k \sin\omega_j}{r_i \Delta\omega},$$

$$\boldsymbol{K}^n_{ijk} = r_i \boldsymbol{H}^n_{ijk} - \frac{\boldsymbol{X}^n_{i+1/2,jk} - \boldsymbol{X}^n_{i-1/2,jk}}{\Delta r_i} - \frac{\boldsymbol{Y}^n_{ij+1/2,k} - \boldsymbol{Y}^n_{ij-1/2,k}}{2\sin(\Delta\omega/2)}.$$

The numerical fluxes through the cell boundaries are determined by the formulas

$$\boldsymbol{X}^n_{i+1/2,jk} = \boldsymbol{g}^n_{i+1/2,jk}\zeta_k \cos\omega_j r_{i+1/2},$$

$$\boldsymbol{Y}^n_{ij+1/2,k} = -\boldsymbol{g}^n_{ij+1/2,k}\zeta_k \sin\omega_{j+1/2}. \tag{24}$$

On the surfaces of the cylinders, we set $\boldsymbol{\delta} \equiv 0$. The distribution function values on the boundaries of the cells $\boldsymbol{g}^n_{i+1/2,jk}$, $\boldsymbol{g}^n_{ij+1/2,k}$, used in the expression for the numerical fluxes (24), are deter-

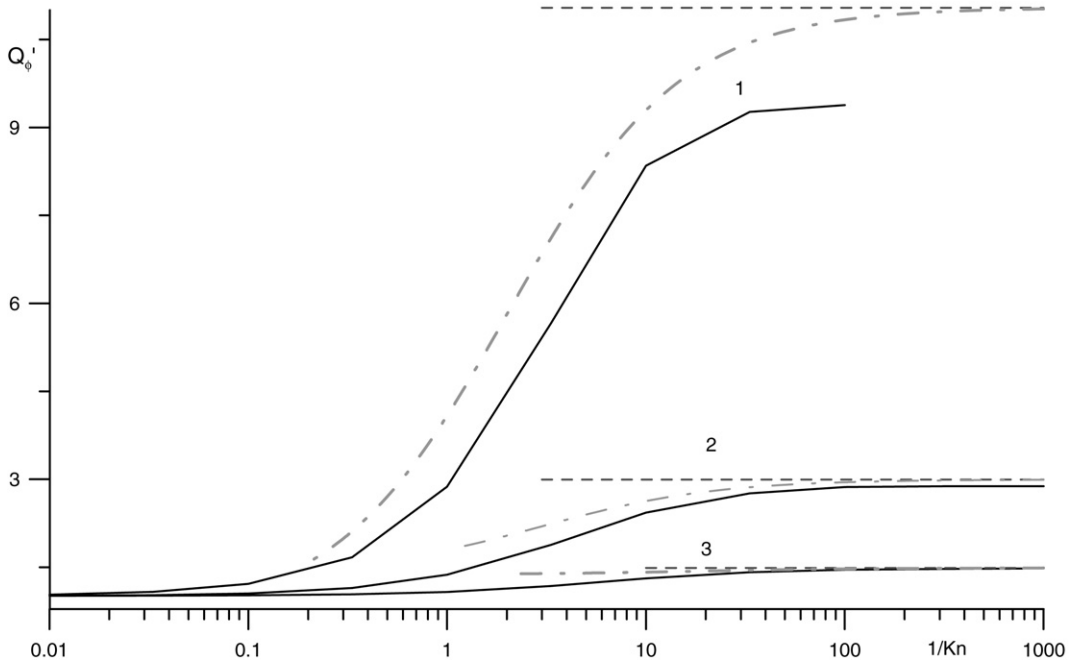

Fig. 11. Normalized mass-flow rate Q'_ϕ for $U_\phi = U_z = 1/2$. Notation is as on Fig. 9.

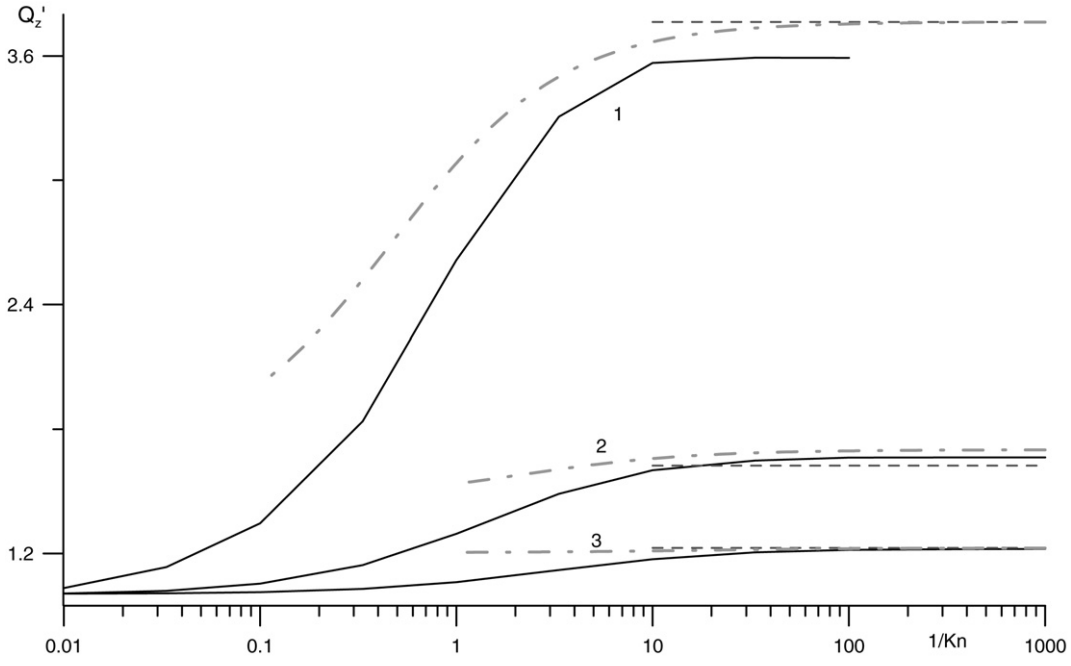

Fig. 12. Normalized mass-flow rate Q'_z for $U_\phi = U_z = 1/2$. Notation is as on Fig. 9.

mined by monotone piecewise-linear interpolation [24,25]. For example, for the spatial fluxes we have

$$\boldsymbol{g}^n_{i+1/2,jk} = \begin{cases} \boldsymbol{g}^n_{ijk} + \dfrac{1}{2}\Delta r_i \operatorname{minmod}(\boldsymbol{D}_{i+1/2,jk}, \boldsymbol{D}_{i-1/2,jk}), \\ \quad \zeta_k \cos\omega_j > 0, \\ \boldsymbol{g}^n_{i+1\,jk} - \dfrac{1}{2}\Delta r_{i+1} \operatorname{minmod}(\boldsymbol{D}_{i+3/2,jk}, \boldsymbol{D}_{i+1/2,jk}), \\ \quad \zeta_k \cos\omega_j < 0 \end{cases} \tag{25}$$

where the vector of slopes $\boldsymbol{D}_{i+1/2,jk}$ is defined as

$$\boldsymbol{D}_{i+1/2,jk} = \frac{\boldsymbol{g}^n_{i+1,jk} - \boldsymbol{g}^n_{ijk}}{r_{i+1} - r_i}.$$

The slope limiter $\operatorname{minmod}(x, y)$ is given by [24,26]

$$\operatorname{minmod}(x, y) = \frac{1}{2}(\operatorname{sign} x + \operatorname{sign} y)\min\bigl(|x|, |y|\bigr)$$

and is applied to each component of the slope vector $\boldsymbol{D}_{i+1/2}$. The use of (25) ensures second-order accuracy on smooth solutions and guarantees that no spurious oscillations occur on discontinuities.

5.2. Calculation of macroscopic parameters

The description of the method is complete once we describe the procedure of computing the macroscopic parameters in the right-hand side. The conventional expressions assume direct approximation of (6) and can be written as

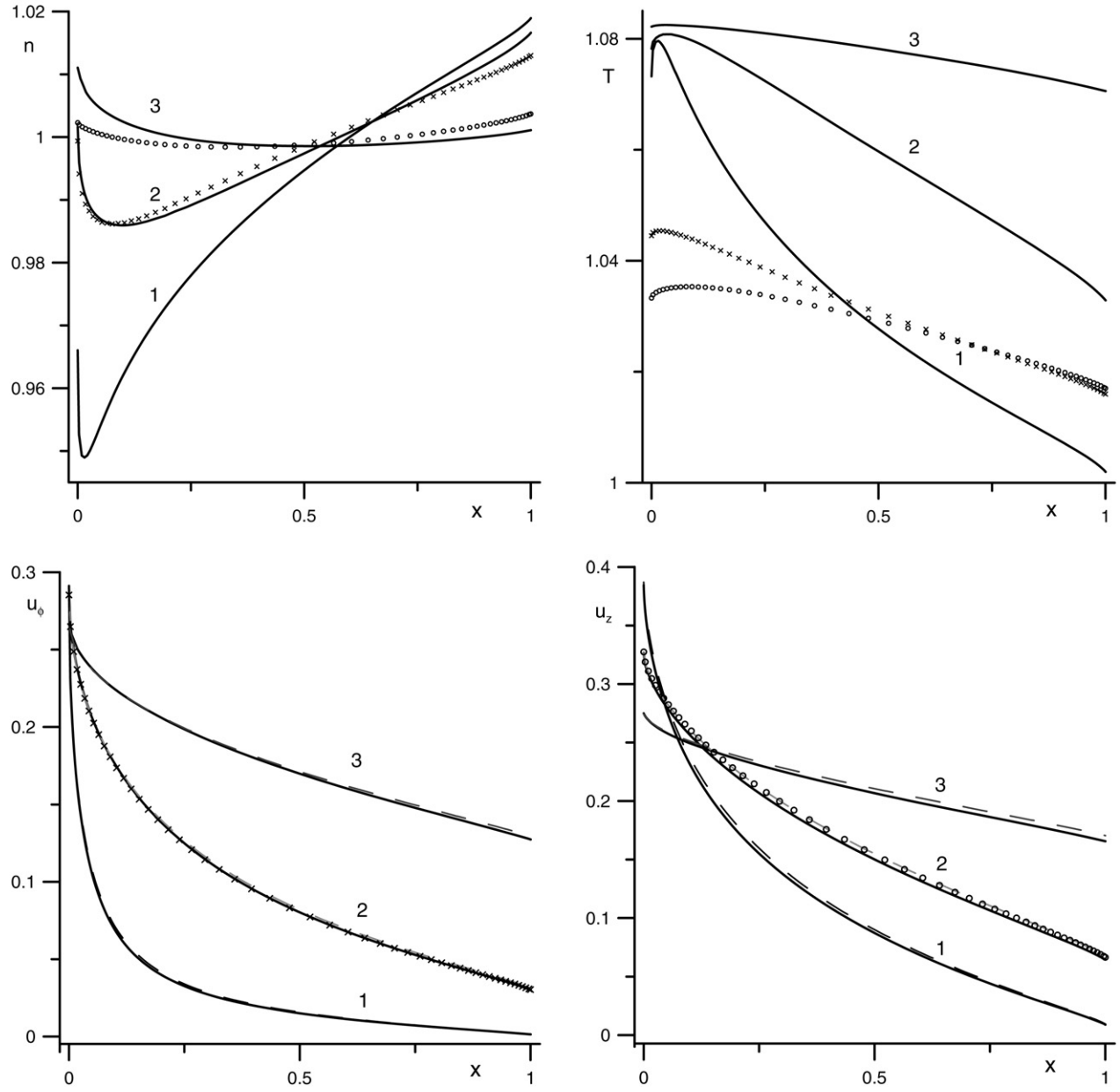

Fig. 13. Macroscopic parameters for $U_\phi = U_z = 1/2$ and $Kn = 1$. Solid line – nonlinear problem, dashed line – linearized solution for gas velocity, circles – pure sliding, crosses – pure rotation. Curves 1, 2, 3 correspond to $\varepsilon = 0.1,\ 0.5,\ 0.9$, respectively.

$$\left(n, nu_\phi, nu_z, \frac{3}{2}nT + nu_\phi^2\right) = \sum_{jk} \left(g_1, \xi_\phi g_1, g_2, \zeta^2 g_1 + g_3\right)_{jk} \zeta_k A_{jk},$$

$$(q_r, q_\phi) = \frac{1}{2} \sum_{jk} (\xi_r, v_\phi)\left[\left(\xi_r^2 + v_\phi^2\right) g_1 + g_2\right]_{jk} \zeta_k A_{jk},$$

$$q_z - nu_z^2 = \frac{1}{2} \sum_{jk} (\xi_r, v_\phi)\left[\left(\xi_r^2 + v_\phi^2\right)(g_2 - u_z g_1) + g_4 - 3u_z g_3\right]_{jk} \zeta_k A_{jk}. \tag{26}$$

Here A_{jk} are the weights of the quadrature formula in the ζ–ω space, which is a tensor product of the composite Simpson rule for integrals with respect to ζ and the second-order accurate midpoint formula involving the distribution function values at the cell centers ω_j.

It can be shown however that the use of (26) results in a method which is not conservative with respect to the collision integral [22], leading to less accurate results. In [23,27] the conservativeness of the method for the S-model equation was ensured by correcting the function $\boldsymbol{g}^+$ in the right-hand side of the kinetic equation. In [28,29] for the simpler Krook model, the gas density, velocity, and temperature were found from a discrete approximation of the conservation laws. For the S-model, however, the conservation laws are insufficient because the heat flux components in $\boldsymbol{g}^+$ remain undetermined.

In the present paper the macroscopic gas parameters, involved in $\boldsymbol{g}_{ijk}$, are determined by a direct approximation of the conditions used in deriving the S-model equation. A detailed explanation of the idea for mona- and diatomic gases can be found in [21,22]. For the present problem this results in the following nonlinear system used for computing macroscopic gas parameters n, u_ϕ, u_z, T, q_r, q_ϕ, q_z at each spatial mesh r_i (index i is omitted for simplicity):

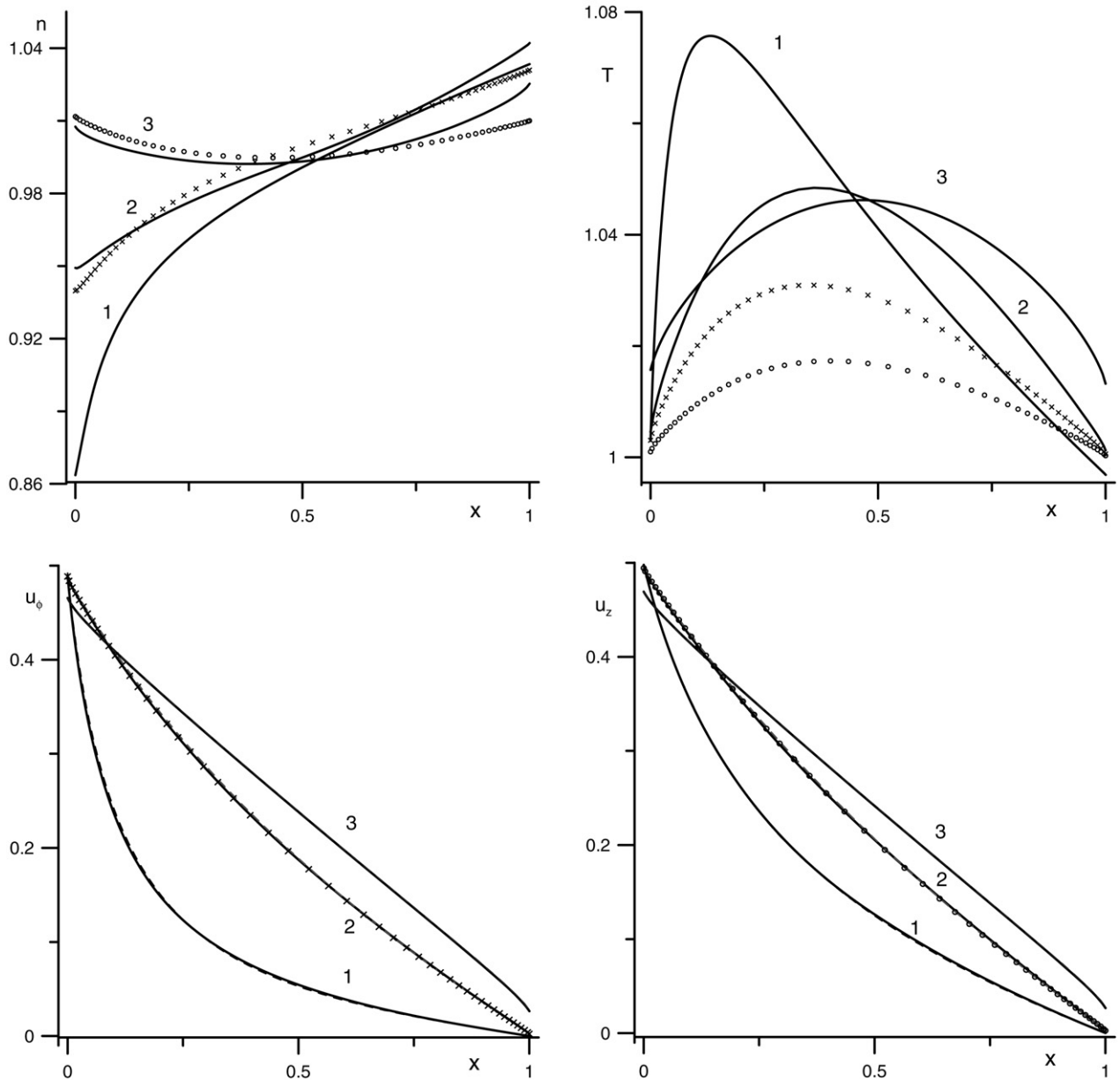

Fig. 14. Macroscopic parameters for $U_\phi = U_z = 1/2$ and $Kn = 0.01$. Notation is as on Fig. 13.

$$\sum_{jk}\left[H_1, H_1\zeta\sin\omega, H_2, \zeta^2 H_1 + H_3\right]_{jk}\zeta_k A_{jk} = \mathbf{0},$$

$$\sum_{jk}(v_\phi, v_r)_{jk}\left[w^2 H_1 - 2u_z H_2 + H_3\right]_{jk}\zeta_k A_{jk} = -(4/3)\nu(q_r, q_\phi),$$

$$\sum_{jk}\left[w^2(H_2 - u_z H_1) + H_4 - 3u_z H_3 + 2u_z^2 H_2 - u_z^3 H_1\right]_{jk}\zeta_k A_{jk} = -(4/3)\nu q_z \tag{27}$$

where $w^2 = v_r^2 + v_\phi^2 + u_z^2$ and the vector $\boldsymbol{H}$ is defined in (21). System (27) is easily solved by Newton's method. As the initial guess we use the values obtained by conventional expressions (26). For $Pr = 1$ our method effectively reduces to [28,29] and can be therefore regarded as its extension.

5.3. Convergence criteria and other remarks

The criterion for the convergence to a steady-state solution is the size of the L_2 norm of the residual $\boldsymbol{R}$ in the steady conservation laws. For the nonlinear equation (21) the components of the residual are determined by numerically integrating the right-hand side of the difference equation with respect to the molecular velocity:

$$\boldsymbol{R}_i = \sum_{jk}\begin{pmatrix} K_1 \\ K_1\zeta\sin\omega \\ K_2 \\ \zeta^2 K_1 + K_3 \end{pmatrix}_{ijk}\zeta_k A_{jk},$$

where the vector $\boldsymbol{K}$ is defined in (22). Note that since the macroscopic parameters are computed by using (27), the integrals of the model collision integrals vanish and we obtain the continuum equations. Usually, the numerical solution was treated as a steady-state one if $\|\boldsymbol{R}\|_{L_2} \leqslant 10^{-4}$.

The resulting numerical method has no time-step restrictions associated with the Courant condition or the approximation of the collision integral and as $t \to \infty$, it approximates the steady kinetic equation to second-order accuracy. The converged steady-state solution satisfies the discrete conservation laws for the density, the z-

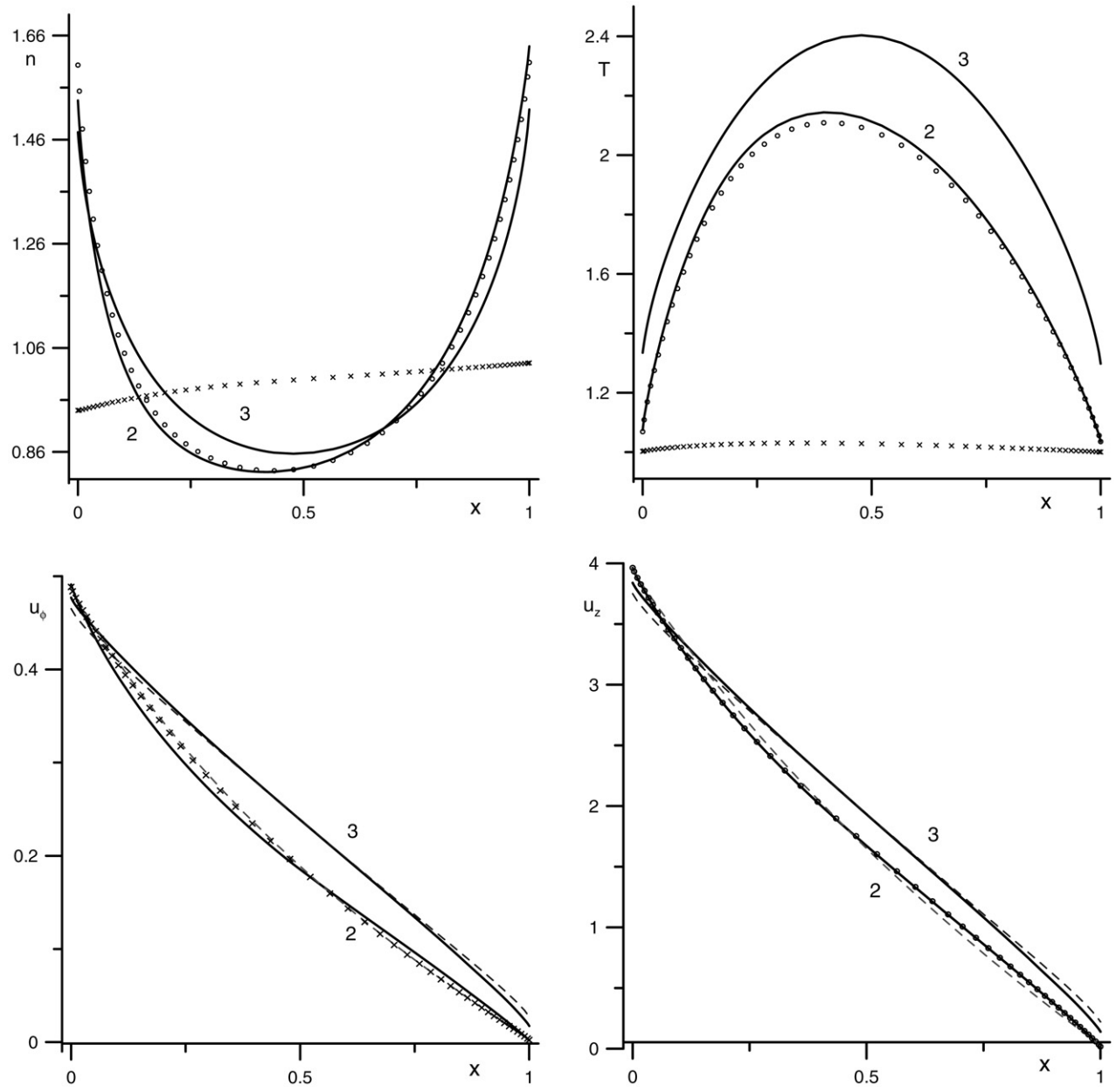

Fig. 15. Macroscopic parameters for $U_\phi = 1/2$, $U_z = 4$ and $Kn = 0.01$. Notation is as on Fig. 14.

component of momentum, and energy. This property follows from the conservativeness of the approximation to the right-hand side of the scheme and from the midpoint formula used for evaluating the integrals with respect to ω.

The numerical method for the linearized equation (16) is constructed in the entirely analogous manner. Details are omitted.

6. Results

The solution of the problem depends on four parameters: Kn, U_ϕ, U_z and ε. For the continuum solution as well as the linearized equations the gas flow is obtained by superposition of longitudinal and rotational motions which depend linearly on the cylinder velocity. In the case of the nonlinear kinetic equation the influences of U_ϕ and U_z cannot in general be separated except in the free-molecular case, in which the longitudinal motion of the cylinder does not affect the flow characteristics corresponding to rotation: u_ϕ, $P_{r\phi}$. The opposite is not true: u_z and P_{rz} depend in a nonlinear way on U_ϕ. One of the aims of the calculations was to study if the above-mentioned properties of the free-molecular solution hold for the finite Knudsen numbers as well.

All the results presented below were obtained for $\mu = \sqrt{T}$ (the hard-sphere law). The calculations were performed for the radius ratios $\varepsilon = r_1/r_2 = 0.1$, 0.5 and 0.9, which correspond to large, moderate, and small widths of the gap between the cylinders, respectively. We note that for $\varepsilon \approx 1$ it is more natural to define the effective Knudsen number as $Kn_1 = \lambda_0/(r_2 - r_1) = \varepsilon\, Kn/(1-\varepsilon)$ whereas in the opposite case $\varepsilon \ll 1$ we can use $Kn_2 = \lambda_0/r_2 = \varepsilon\, Kn$ so that

$$Kn_2 \ll Kn \ll Kn_1. \tag{28}$$

We remark that from the point of view of compressible gas dynamics the cylindrical Couette flow in the case of pure rotation of the inner cylinder becomes unstable for sufficiently small Knudsen numbers and no steady solution exists. It is not entirely clear to which extent this result can be applied to the present flow of a rarefied gas. The linear stability of the purely rotational cylindrical Couette flow of a rarefied gas was recently investigated in

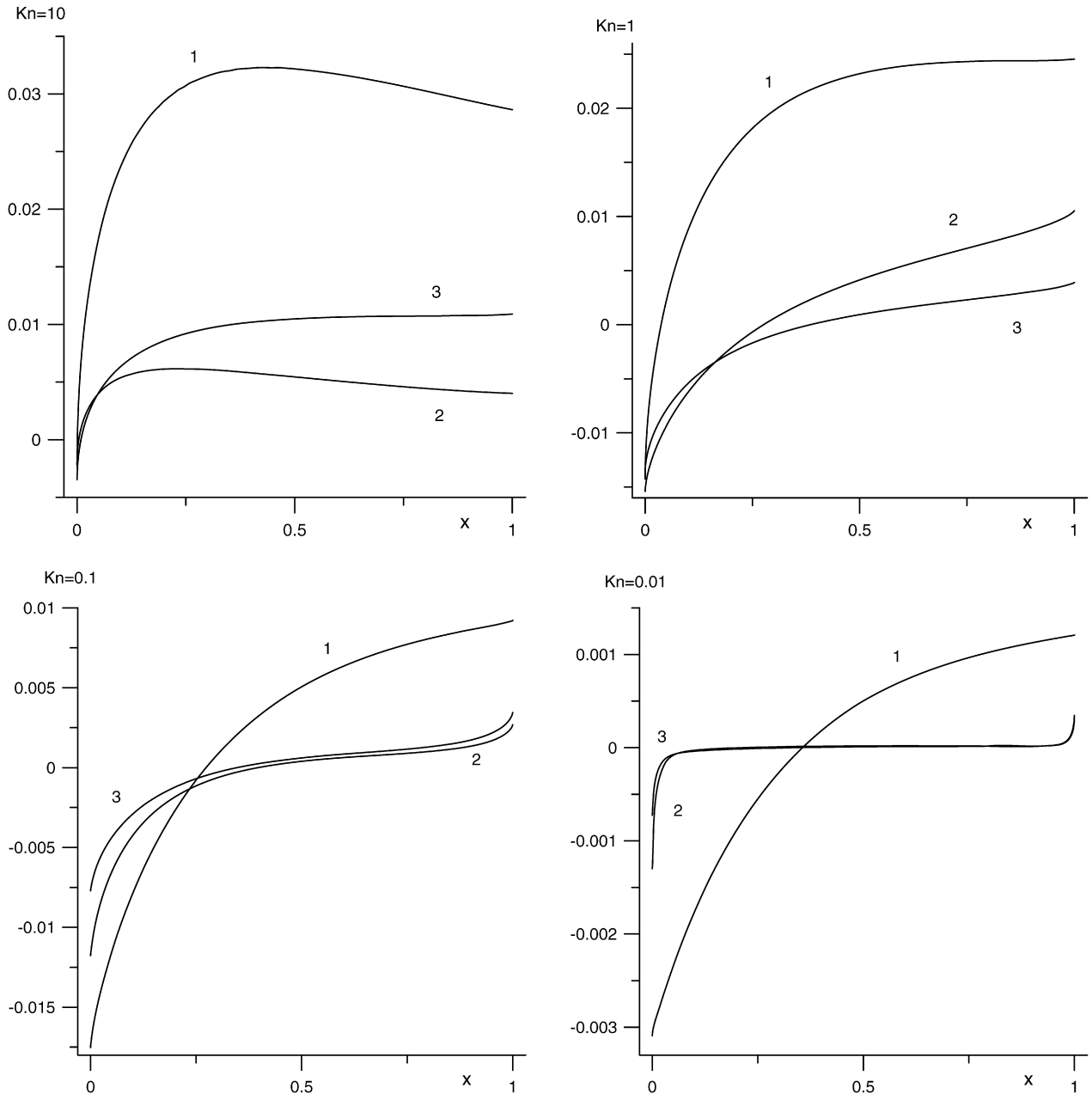

Fig. 16. Heat fluxes for $U_\phi = U_z = 1/2$, $\varepsilon = 1/2$ and different Knudsen numbers. Curves 1, 2, 3 correspond to q_r, q_ϕ and q_z, respectively.

[30]. Here we assume that the flow is steady in the entire range of Knudsen numbers used in the calculations.

6.1. Shear stresses and mass-flow rates

We begin our analysis by studying the behavior normalized shear stresses A', B' and mass-flow rates Q'_ϕ, Q'_z, which are defined as the ratio of the actual value for a given Knudsen number to its free-molecular limit. Figs. 1–4 illustrate the dependence of shear stresses and mass flow rates on Kn for different values of U_ϕ and U_z. The solid lines depict the general case $U_\phi = U_z = 1/2$. Curves 1, 2, 3 correspond to the solution of the nonlinear kinetic equation (5) for $\varepsilon = 0, 1, 0.5, 0.9$, respectively. For the particular value $\varepsilon = 1/2$ we also plot by circles the profiles of A', Q'_ϕ for purely rotation ($U_z = 0$) and B', Q'_z for purely longitudinal movements of the inner cylinder ($U_\phi = 0$). Tables 1, 2 contain the actual values for the particular case $\varepsilon = 1/2$, $U_\phi = U_z = 1/2$, obtained by solving the linearized and nonlinear kinetic equations, respectively. We also tabulate the errors in fulfilling the conditions (8) defined as

$$\delta_A = \max_i |A_i/A_1 - 1|, \qquad \delta_B = \max_i |B_i/B_1 - 1|,$$
$$\delta_C = \max_i |C_i/C_1 - 1|. \tag{29}$$

We see that overall the solution of the problem depends strongly on the ratio of cylinder radiuses ε. Interestingly, with a good accuracy the normalized shear stresses have the following properties:

$$A'(Kn, \varepsilon, U_\phi, U_z) = A'(Kn, \varepsilon, U_\phi, 0),$$
$$B'(Kn, \varepsilon, U_\phi, U_z) = B'(Kn, \varepsilon, 0, U_z). \tag{30}$$

Moreover, there is a good agreement with the linearized solution in the whole range of the Knudsen numbers. The continuum

Table 1
Linearized solution for $\varepsilon = 1/2$

Kn	A'	Q'_ϕ	B'	Q'_z	δ_A	δ_B
100	0.99746	1.01020	0.99652	1.00680	0.9704	0.0549
10	0.98794	1.04862	0.97024	1.05208	0.9205	0.0536
1	0.89096	1.37193	0.75969	1.27393	0.5709	0.0448
0.1	0.37793	2.44801	0.22641	1.56183	0.0971	0.0416
0.01	0.05045	2.87012	0.02754	1.61527	0.6834	0.7286
0.001	0.00524	2.87953	0.00283	1.61592	4.2159	4.2230

Table 2
Normalized shear stresses and mass-flow rates for the generalized Couette flow with $\varepsilon = 1/2$, $U_z = U_\phi = 1/2$

Kn	A'	Q'_ϕ	B'	Q'_z	δ_A	δ_B	δ_C
100	0.99725	1.01048	0.99645	1.00591	1.0054	0.0455	0.2095
10	0.98890	1.04979	0.97199	1.05467	0.9589	0.0420	0.2097
1	0.89101	1.37107	0.76355	1.29503	0.6146	0.0504	0.2497
0.1	0.37530	2.42876	0.22657	1.60214	0.1383	0.0930	0.4572
0.01	0.05060	2.86795	0.02763	1.66287	1.3834	0.8481	1.9057
0.001	0.00538	2.87961	0.00286	1.66389	6.6706	5.8933	6.3792

Table 3
Normalized shear stresses and mass-flow rates for the generalized Couette flow with $\varepsilon = 1/2$, $U_z = 4$, $U_\phi = 1/2$

Kn	Results				Errors		
	A'	Q'_ϕ	B'	Q'_z	δ_A	δ_B	δ_C
100	1.00547	1.02477	1.00298	1.01119	1.7685	0.0750	0.0792
30	1.02017	1.04421	1.01035	1.02775	1.7097	0.0752	0.0795
10	1.05228	1.09126	1.02189	1.06500	1.5707	0.0754	0.0803
3	1.10215	1.20336	1.00932	1.13921	1.2458	0.0722	0.0782
1	1.08895	1.39496	0.88828	1.23205	0.7318	0.0653	0.0735
0.3	0.87598	1.80914	0.59146	1.36899	0.1404	0.0844	0.0971
0.1	0.50904	2.33271	0.29824	1.50889	0.3011	0.2600	0.3104
0.03	0.18902	2.66396	0.10393	1.59310	0.8722	1.7805	2.1666
0.01	0.06435	2.74987	0.03398	1.61656	3.9625	7.4267	9.1973

Table 4
Normalized shear stresses and mass-flow rates for the generalized Couette flow with $\varepsilon = 1/2$, $U_z = 7$, $U_\phi = 1/2$

Kn	Results				Errors		
	A'	Q'_ϕ	B'	Q'_z	δ_A	δ_B	δ_C
100	1.01642	1.03369	1.01226	1.01418	1.7545	0.0748	0.0762
30	1.05307	1.06659	1.03759	1.03663	1.6759	0.0754	0.0768
10	1.13098	1.13520	1.08380	1.07751	1.5102	0.0756	0.0773
3	1.25807	1.25055	1.11990	1.12615	1.1258	0.0738	0.0758
1	1.30722	1.38021	1.02926	1.15630	0.5441	0.0718	0.0740
0.3	1.12023	1.71783	0.73677	1.26054	0.0947	0.1283	0.1338
0.1	0.68319	2.23929	0.39314	1.42865	0.3493	0.8229	0.8714
0.03	0.24989	2.58048	0.13348	1.54037	4.1736	7.8059	8.3036

solution is close to the kinetic one for small effective Knudsen numbers, defined in (28). Dependence of mass flow rate on the cylinder movement is more complex. Similar to shear stresses, the normalized mass-flow in the azimuthal direction Q'_ϕ is not influenced by the value of U_z; nonlinear and linearized solutions agree reasonably well. However, the normalized mass-flow rate in the longitudinal direction Q'_z depends on the rotation velocity of the inner cylinder, especially for small ε and Kn. Since in the linearized problem rotation and longitudinal movement of the cylinder do not influence each other, the linearized solution for Q'_z coincides with the nonlinear solution in the case $U_\phi = 0$ but differs from the nonlinear solution for the spiral movement. We also note, that the normalized mass-flow rates seem to approach a limiting value as $Kn \to 0$ (within the numerical accuracy) for both linearized and nonlinear solutions.

The increase of U_z leads to strong nonlinearity of the solution. Figs. 5, 6 illustrate the same quantities as in Figs. 1–4 but for $U_z = 4$, $U_\phi = 1/2$. Values of normalized mass-flow rates and shear stresses are given in Table 3. The most significant difference from the previous case is the appearance of the stress maximum effect in both longitudinal and azimuthal directions: with decrease in the Knudsen number, A', B' first increase and then begin to fall. We remark that for the plane Couette flow the stress maximum effect was first observed in [18]. The appearance of the stress-maximum effect in the azimuthal direction shows a rather strong coupling of rotation and longitudinal movements in the nonlinear problem. Recall, that for $U_\phi = U_z = 1/2$ the longitudinal movement of the inner cylinder virtually does not affect the stress and mass-flow rate in azimuthal direction. Interestingly, the maximum in A' is much more pronounced than in B' and is achieved for smaller Knudsen numbers. Further increase in U_z leads to a more pronounced stress-maximum effect, see Table 4. The calculated value of A' exceeds its free-molecular value by approximately 30%.

On the other hand, the normalized mass-flow rates in both longitudinal and azimuthal directions decrease with growing U_z. Note, that in the free-molecular case the actual (not normalized) value of Q_ϕ does not depend on U_z, whereas Q_z is a linear function of U_z. See Eq. (9). Therefore, the increase in U_z leads to the moderate decrease in the azimuthal mass-flow rate and a large increase in the longitudinal mass-flow rate.

The general nonlinear solution for shear stresses differs from both linearized and purely rotational/longitudinal movement at all Knudsen numbers. On the other hand, the dependencies of the mass flow rates on Kn and ε, shown in Figs. 5, 6 are qualitatively similar to those plotted in Figs. 1–4 and for $\varepsilon \geqslant 1/2$ agree well with the linearized solution, even though the velocity of the inner cylinder is large.

Table 5
Average velocities for the generalized Couette flow with $\varepsilon = 0.9$

Kn		100	10	1	0.1	0.01	0.001
Lin. sol.,	W_ϕ/U_ϕ	0.33034	0.33250	0.35119	0.42719	0.47456	0.48072
	W_z/U_z	0.40347	0.40613	0.42450	0.46537	0.48053	0.48223
$U_z = U_\phi = \frac{1}{2}$	W_ϕ/U_ϕ	0.32792	0.33014	0.34898	0.42406	0.47236	0.47876
	W_z/U_z	0.39552	0.39832	0.41760	0.46108	0.47862	0.48068
$U_z = 4$, $U_\phi = \frac{1}{2}$	W_ϕ/U_ϕ	0.32816	0.3325	0.36062	0.43056	0.47054	0.47678
	W_z/U_z	0.39575	0.4004	0.42519	0.45900	0.47562	0.47998

Average flow velocities for $\varepsilon = 0.9$ are tabulated in Table 5. We observe that as the Knudsen number decreases, both velocities approach the values $U_\phi/2$, $U_z/2$, respectively, which are predicted by the classical Couette flow between parallel plates. The same applies to the continuum solution. We also note that for all Knudsen numbers the average velocities depend almost linearly on the velocity of the inner cylinder and thus can be computed accurately from the solution of the linearized problem with reasonable accuracy.

Figs. 9, 10 show the comparisons of normalized shear stresses from the solution of the nonlinear kinetic equation and the incompressible continuum solution with both types of the boundary conditions. Overall, reasonable agreement is observed for sufficiently small Kn numbers only. The use of the velocity–slip boundary conditions gives only moderate improvement for all cases except the B' profile for $\varepsilon = 0.9$. For the latter case the continuum solution (13) is surprisingly accurate in the entire range of Knudsen numbers. Figs. 11, 12 show the results for normalized mass flow rates. Reasonable agreement exists for small Kn numbers and not very small values of ε. As before, the use of the velocity–slip boundary conditions improves the results somewhat, most visibly for $\varepsilon = 0.1$, but the quantitative error for moderate and high Knudsen numbers remains large.

We have also carried out a comparative study for the case of the large sliding velocity of the inner cylinder. The overall outcome of this study is very similar to the case of $U_\phi = U_z = 1/2$. In par-

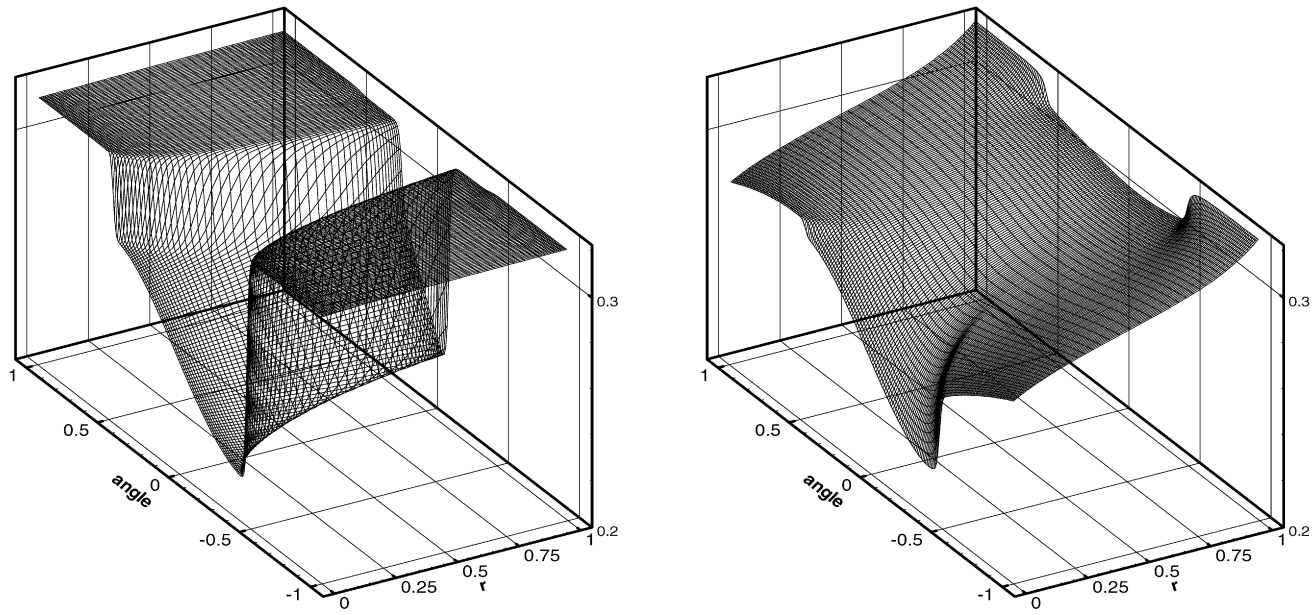

Fig. 17. Generalized movement of the inner cylinder with $U_\phi = U_z = 1/2$. $r-\omega$ plots of g_1 for $\zeta = 1/8$, $Kn = 100$ (left) and $Kn = 1$ (right).

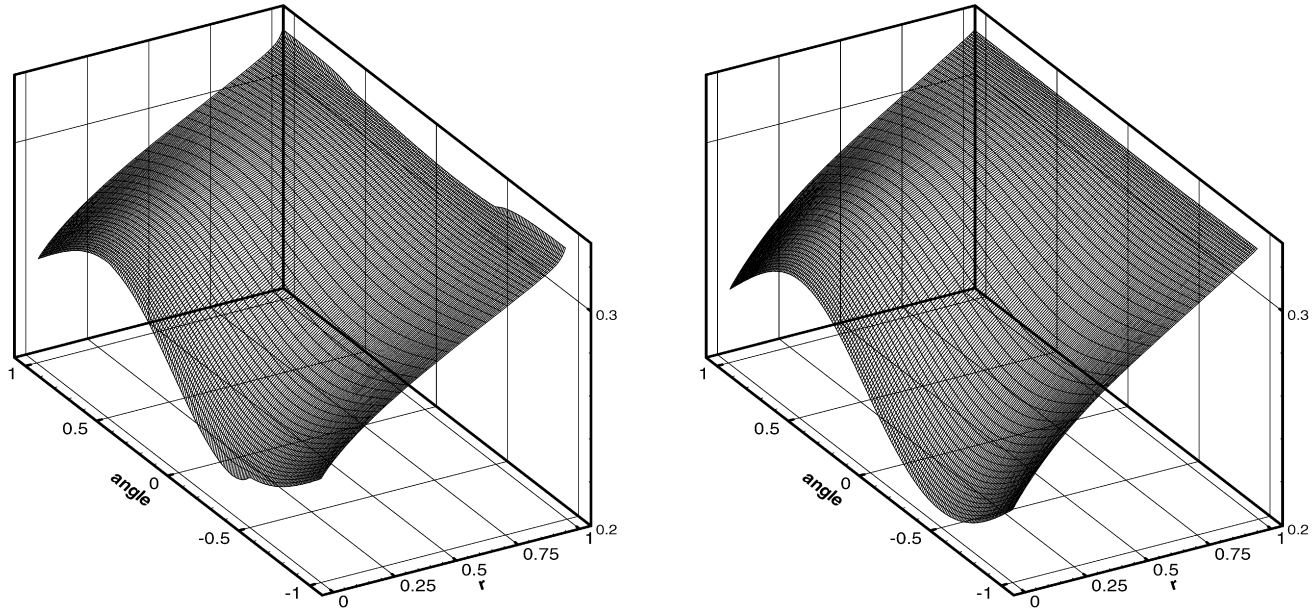

Fig. 18. Generalized movement of the inner cylinder with $U_\phi = U_z = 1/2$. $r-\omega$ plots of g_1 for $\zeta = 1/8$, $Kn = 0.1$ (left) and $Kn = 0.01$ (right).

ticular, the highly nonlinear stress maximum effect is not captured at all by the continuum equations. The results are omitted.

6.2. Macroscopic parameters

We now study the dependence of gas macroscopic parameters on ε and movement of the inner cylinder. Fig. 13 illustrates the distributions of density, velocities and temperature as functions of reduced spatial coordinate $x = (r - r_1)/(r_2 - r_1)$ for $Kn = 1$, $U_z = 1/2$, $U_\phi = 1/2$ and different ε, obtained by solving both nonlinear and linearized kinetic equations Solid lines correspond to the solution of the nonlinear kinetic equation, circles show the case of pure rotation, triangles – pure longitudinal flow. Curves 1, 2, 3 correspond to $\varepsilon = 0.1$, 0.5, 0.9. We can see a strong dependence of the profiles on ε as well as on the type of the cylinder movement. The gas velocity is not sensitive to the latter factor; the linearized solution for velocity agrees well with the nonlinear one.

Fig. 14 illustrates the distributions of density, velocities and temperature fir $Kn = 0.01$; all other parameters are the same as on Fig. 13. Similar to Fig. 13, the main observation is that all macroscopic quantities depend strongly on ε. Density and temperature are also very sensitive to the type of the movement of the inner cylinder. We again see good agreement between the nonlinear and linearized solutions.

Fig. 15 depicts density, velocities and temperature of the gas for the case of large sliding velocity of the inner cylinder $U_z = 4$, $U_\phi = 1/2$ and a small Knudsen number $Kn = 0.01$. We see that the density and temperature distributions are almost entirely defined by the value of $U_z > 1$; the influence of rotation of the inner cylinder is small. On the other hand, the qualitative behavior of velocity profiles coincides completely with that shown on Figs. 14 for $U_z = U_\phi = 1/2$ and is well described by the linearized equation.

Fig. 16 shows the behavior of heat fluxes for different Knudsen numbers for the case $U_\phi = U_z = 1/2$, $\varepsilon = 1/2$. We see that the

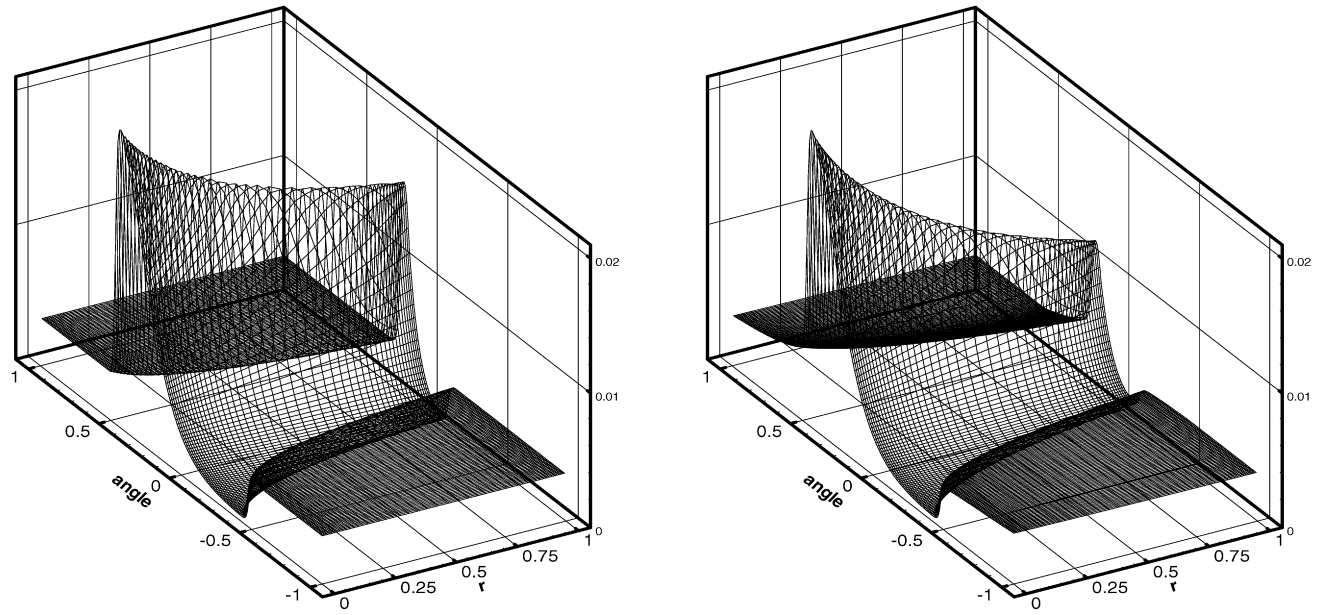

Fig. 19. Generalized movement of the inner cylinder with $U_\phi = U_z = 1/2$. $r-\omega$ plots of g_1 for $\zeta = 2.125$, $Kn = 100$ (left) and $Kn = 1$ (right).

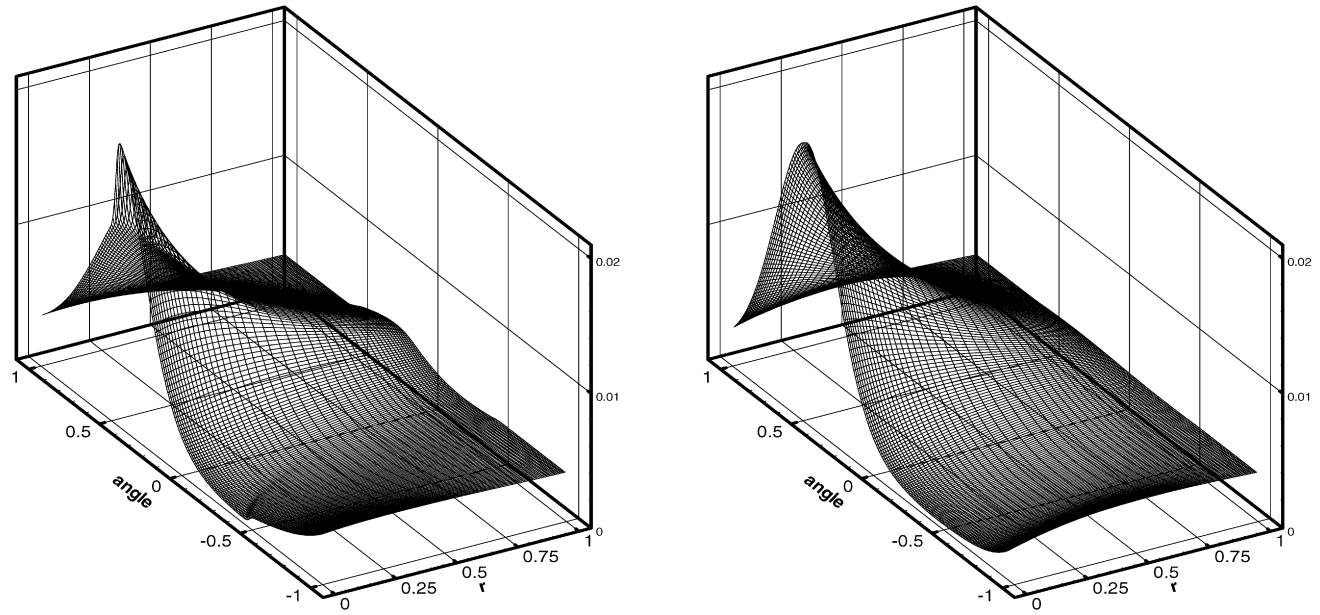

Fig. 20. Generalized movement of the inner cylinder with $U_\phi = U_z = 1/2$. $r-\omega$ plots of g_1 for $\zeta = 2.125$, $Kn = 0.1$ (left) and $Kn = 0.01$ (right).

heat flux in the radial direction is the largest whereas two other fluxes are much smaller and diminish rapidly as Kn decreases; for $Kn = 0.01$ they are visible only in the Knudsen layers near the surfaces.

We have also found that the type of movement of the inner cylinder (general, pure sliding or pure rotation) influences all three components of the heat flux quite significantly. The corresponding results are omitted to save space.

6.3. Velocity distribution function

We now study the influence of the Knudsen number on the velocity distribution function. We first consider the case of moderate values of both velocity of the inner cylinder $U_z = U_\phi = 1/2$ and ratio of cylinder radiuses $\varepsilon = 1/2$. On Figs. 18–20 we plot the surface of $g_1(r, \zeta, \phi)$ for $\zeta = 0.125$, 2.125 and a sequence of Knudsen numbers $Kn = 100$, 1, 0.1 and 0.01. While studying these plots it is important to remember that the decay of discontinuities of the of the velocity distribution functions is proportional to $\exp(-s/s_*)$, where s is the coordinate along the characteristic and $s_* = \zeta/\nu \sim \zeta\, Kn$. Therefore, for large ζ (fast molecules) the discontinuities decay much slower than for small ζ (slow molecules).

As is expected, for the large Knudsen number $Kn = 100$ the discontinuities of the velocity distribution dominate; it is also clear that the behavior of g_1 depends quite strongly on ζ. As the Knudsen number is decreased to the transitional value $Kn = 1$, the distribution function is almost smooth for small ζ. For large ζ the discontinuities are still present but decay with r. Finally, for $Kn = 0.1$ and $Kn = 0.01$ the distribution function appears to be smooth for all ζ; we also see the formation of the boundary layer close to the surface of the inner cylinder; it is however quite small for the given value of U_z.

As the sliding velocity of the inner cylinder increases, the qualitative behavior of the distribution function does not change with one exception: for small *Kn* we observe the formation of a stronger boundary layer near the inner cylinder. The results are omitted.

7. Conclusions

We have studied the cylindrical Couette flow of a rarefied gas in the generalized formulation when the inner cylinder not only rotates but also slides along its axis. Our study included the analysis of the limiting cases in which the linearized kinetic equation or incompressible Navier–Stokes equations apply. For arbitrary Knudsen numbers or large velocities the problem has been studied on the basis of the full nonlinear model kinetic equation by using a second order accurate non-oscillatory method, conservative with respect to the collision integral.

We have analyzed the influence of four main problem parameters: Knudsen number, cylinder velocities as well as ratio of radiuses on shear stresses, mass flow rates and distribution of macroscopic parameters. The main results can be summarized as follows:

- The flow pattern depends strongly on the ratio of cylinder radiuses and the velocity of the inner cylinder.
- For moderate velocity of the inner cylinder shear stresses and mass flow rates in the azimuthal direction do not depend on the longitudinal movement.
- For large longitudinal velocities of the inner cylinder a stress maximum effect is observed not only in the longitudinal direction, but also in the azimuthal one despite the fact that the rotational velocity remains relatively small.
- The increase in the longitudinal velocity of the inner cylinder influences the normalized mass-flow rates in both longitudinal and azimuthal directions.
- The range of applicability of linearized and continuum solutions has been identified for both integral quantities and macroscopic variables.
- The behavior of the velocity distribution function depends significantly on Knudsen numbers and molecular velocities.

Acknowledgements

The authors would like to thank one of the anonymous referees for important remarks concerning the formulation of the linearized problem. The first author acknowledges the partial support of the Russian Foundation for Basic Research (project No. 04-01-00347). The second author acknowledges the financial support provided by the PRIN programme (2004–2006) of Italian Ministry of Education and Research (MIUR). He would also like to thank Professor E.F. Toro OBE for numerous discussions on the construction of the Godunov-type methods.

References

[1] T. Soga, H. Oguchi, A nonlinear analysis of cylindrical Couette flow, in: Rarefied Gas Dynamics, Proc. 9th Int. Symp., DFVLR Press, Porz-Wahn, Germany, 1974. Paper No. A. 17.
[2] K. Nanbu, Analysis of cylindrical Couette flows by use of the direct simulation method, Phys. Fluids 27 (11) (1984) 2632–2635.
[3] F.M. Sharipov, G.M. Kremer, Non-isothermal Couette flow of a rarefied gas between two rotating cylinders, Eur. J. Mech. B/Fluids 18 (1) (1999) 121–130.
[4] K. Aoki, H. Yoshida, T. Nakanishi, Inverted velocity profile in the cylindrical Couette flow of a rarefied gas, Phys. Rev. E 68 (2003) 016302.
[5] V.A. Titarev, E.M. Shakhov, Kinetic analysis of longitudinal Couette flow between coaxial cylinders, Fluid Dynam. 41 (1) (2006) 86–99.
[6] E.M. Shakhov, Approximate kinetic equations in rarefied gas theory, Fluid Dynam. 3 (1) (1968) 156–161.
[7] E.M. Shakhov, Generalization of the Krook kinetic relaxation equation, Fluid Dynam. 3 (5) (1968) 142–145.
[8] V.A. Titarev, E.M. Shakhov, Numerical analysis of the spiral Couette flow of a rarefied gas between coaxial cylinders, Comput. Math. Math. Phys. 46 (3) (2006) 503–513.
[9] C.K. Chu, Kinetic-theoretic description of the formation of a shock wave, Phys. Fluids 8 (1) (1965) 12–22.
[10] A.M. Bishaev, V.A. Rykov, Solution of steady kinetic problems at moderate and small Knudsen numbers, USSR Comp. Math. Math. Phys. 15 (1) (1975) 172–182.
[11] N.E. Kochin, I.A. Kibel, N.N. Rose, Theoretical Hydromechanics, vol. 2, Fizmatgiz, 1963 (in Russian).
[12] V.P. Shidlovskiy, Cylindrical Couette flow in a weakly rarefied gas, Engrg. J. 4 (4) (1964).
[13] S.A. Schaaf, Mechanics of rarefied gases, in: Encyclopedia of Physics, vol. VIII/2, Springer-Verlag, Berlin, 1963, pp. 591–696.
[14] M.N. Kogan, Rarefied Gas Dynamics, Plenum, New York, 1969.
[15] M.N. Kogan, Kinetic theory in aerothermodynamics, Prog. Aerospace Sci. 29 (1992) 271–354.
[16] T. Ohwada, Y. Sone, K. Aoki, Numerical analysis of the shear and thermal creep flows of a rarefied gas over a plane wall on the basis of the linearized Boltzmann equation for hard sphere molecules, Phys. Fluids A 1 (12) (1989) 2042–2049.
[17] Y. Sone, S. Takata, T. Ohwada, Numerical analysis of the plane Couette flow of a rarefied gas on the basis of the linearized Boltzmann equation for hard-sphere molecules, Eur. J. Mech. B/Fluids 9 (3) (1990) 273–288.
[18] E.M. Shakhov, Couette problem for the generalized Krook equation. Stress-peak effect, Fluid Dynam. 4 (5) (1969) 9–13.
[19] M.Ya. Ivanov, R.Z. Nigmatullin, Implicit scheme of S.K. Godunov with increased order of accuracy for Euler equations, USSR Comp. Math. Math. Phys. 27 (11) (1987) 1725–1735.
[20] J.Y. Yang, J.C. Huang, Rarefied flow computations using nonlinear model Boltzmann equations, J. Comput. Phys. 120 (2) (1995) 323–339.
[21] V.A. Titarev, E.M. Shakhov, Numerical calculation of the hypersonic rarefied transverse flow past a cold flat plate, Fluid Dynam. 40 (5) (2005) 790–804.
[22] V.A. Titarev, Conservative numerical methods for model kinetic equations, Computers and Fluids 36 (9) (2007) 1446–1459.
[23] I.N. Larina, V.A. Rykov, A numerical method for calculating axisymmetric rarefied gas flows, Comput. Math. Math. Phys. 38 (8) (1998) 1335.
[24] V.P. Kolgan, Application of the minimum-derivative principle in the construction of finite-difference schemes for numerical analysis of discontinuous solutions in gas dynamics, Trans. Central Aerohydrodynamics Institute 3 (6) (1972) 68–77 (in Russian).
[25] V.P. Kolgan, Finite-difference schemes for computation of three dimensional solutions of gas dynamics and calculation of a flow over a body under an angle of attack, Trans. Central Aerohydrodynamics Institute 6 (2) (1975) 1–6 (in Russian).
[26] N.I. Tillaeva, A generalization of the modified Godunov scheme to arbitrary unstructured meshes, Trans. Central Aerohydrodynamics Institute 17 (2) (1986) 18–26 (in Russian).
[27] M.I. Gradoboev, V.A. Rykov, Conservative method for numerical solution of the kinetic equations for small Knudsen numbers, Comput. Math. Math. Phys. 34 (2) (1994) 246–266.
[28] L. Mieussens, Discrete-velocity models and numerical schemes for the Boltzmann-BGK equation in plane and axisymmetric geometries, J. Comput. Phys. 162 (2) (2000) 429–466.
[29] A.V. Gusarov, I. Smurov, Gas-dynamic boundary conditions of evaporation and condensation: numerical analysis of the Knudsen layer, Phys. Fluids 14 (12) (2002) 4242–4255.
[30] H. Yoshida, K. Aoki, Linear stability of the cylindrical Couette flow of a rarefied gas, Phys. Rev. E 73 (2006) 021201.